DERIVATION OF HIGHER ORDER GRADIENT CONTINUUM MODELS FROM ATOMISTIC MODELS FOR CRYSTALLINE SOLIDS[*]

M. ARNDT[†] AND M. GRIEBEL[†]

Abstract. We propose a new upscaling scheme for the passage from atomistic to continuum mechanical models for crystalline solids. It is based on a Taylor expansion of the deformation function and allows us to capture the microscopic properties and the discreteness effects of the underlying atomistic system up to an arbitrary order. The resulting continuum mechanical model involves higher order terms and gives a description of the specimen within the quasi-continuum regime. Furthermore, the convexity of the atomistic potential is retained, which leads to well-posed evolution equations. We numerically compare our technique to other common upscaling schemes for the example of an atomic chain. Then we apply our approach to a physically more realistic many-body potential of crystalline silicon. Here the above-mentioned advantages of our technique hold for the newly obtained macroscopic model as well.

Key words. continuum limit, quasi-continuum approximation, upscaling, multiscale simulation, molecular dynamics, continuum mechanics, higher order gradient, hyperbolic, silicon

AMS subject classifications. 35L75, 65M06, 70F10, 74B20, 82C21

DOI. 10.1137/040608738

1. Introduction. The behavior of material often involves quite different length scales. Therefore mathematical models on different length scales have also been derived. To this end, macroscopic effects can often be well described on the continuum mechanical level. Here the stored energy density $\Phi^{(C),x} : \mathbb{R}^{d \times d} \to \mathbb{R}$ of a solid at a point x is usually assumed to be a function of the deformation gradient $F = \nabla y(x)$, where $y : \Omega \to \mathbb{R}^d$ denotes the deformation function of the solid and $\Omega \subset \mathbb{R}^d$ describes the reference configuration. This leads to the overall energy

$$(1.1) \qquad \Phi^{(C)}(y) = \int_\Omega \Phi^{(C),x}(\nabla y(x)) \, dx.$$

On the other hand, the solid can be described on the atomic level by a system of interacting atoms. Such a model then includes microscopic effects, which give a more accurate characterization of the solid on a finer length scale. However, the simulation of the behavior on a coarse length scale usually cannot be performed for the atomistic model due to computational limits. Therefore the question arises of how a macroscopic description on the continuum mechanical level can be derived from a microscopic description on the atomic level.[1]

One approach for the passage from the atomic to the continuum level is given by the so-called scaling technique. Here the atomistic potential $\Phi^{(A)}(\cdot)$ is scaled as

$$(1.2) \qquad \varepsilon^d \Phi^{(A)}(\varepsilon^{-1} \cdot),$$

[†]Institute for Numerical Simulation, University of Bonn, Germany (arndt@ins.uni-bonn.de, griebel@ins.uni-bonn.de).

[1]The atomic level is by far not the finest level on which a solid can be modeled. The atomistic model should itself be rigorously derived from a quantum mechanical model. To this end, a whole hierarchy of scales could be studied. In this article, we focus on the relation between the atomic and the continuum mechanical level only.

where $\varepsilon > 0$ gives the characteristic length. The limit $\varepsilon \to 0$ then leads to a continuum mechanical energy $\Phi^{(C)}$ of the form (1.1). This approach has been studied by Blanc, Le Bris, and Lions [5], E and Huang [16], and others.

For the continuum mechanical model which is obtained by the scaling technique, the evolution is governed by the nonlinear wave equation

$$(1.3) \qquad \rho \frac{\partial^2 y}{\partial t^2} = \operatorname{div} \Phi^{(C),x'}(\nabla y),$$

where ρ is the mass density and $\Phi^{(C),x'}$ denotes the first derivative of the potential energy density of the system. From the view of continuum mechanics, $\Phi^{(C),x'}$ describes the stress. It is well known that the solution of such nonlinear hyperbolic equations typically exhibits shocks after finite time. Furthermore, these equations then possess no classical solutions, even for smooth initial data; see, e.g., [12]. Only solutions in a weaker sense exist. This breakdown of the solution theory is in contrast to the discrete system, which admits a solution for an infinite time horizon. The reason for this is the discreteness of the atomistic system. It leads to a certain dispersion which has a regularizing effect. This dispersion is not contained in the continuum model, because the scaling technique describes the full continuum limit. It drives the number N of atoms to infinity and therefore destroys all discreteness effects.

On the macroscale, further terms are often added to the continuum model, mostly higher order contributions to the potential energy such as $|\nabla^2 y|^2$. This regularizes the problem as well. Also, further physical effects such as surface contributions or the determination of the length scale can be captured phenomenologically in this way; see, e.g., [3] for an example in the context of shape memory alloys. But these additional terms are somewhat artificial. They are often chosen phenomenologically and are not deduced from the atomistic model.

Higher order contributions in continuum mechanics have been used already in 1893 by Van der Waals (see [34] and [27] for the English translation) to describe capillarity effects of fluids. In the context of elasticity theory of solids, they have been studied, e.g., by Bardenhagen and Triantafyllidis [4] and Triantafyllidis and Bardenhagen [32, 33]. The so-called gradient theory developed by Aifantis [2] postulates a relationship of stress and strain in terms of higher order derivatives for elasticity, plasticity, and dislocation dynamics problems. A systematic way to derive higher order terms is given by the so-called direct expansion technique. It has first been proposed by Kruskal and Zabusky [23] and Zabusky and Kruskal [37] and was further developed by Rosenau [24] and Collins [10]. Numerical investigations have been performed by Kevrekidis et al. [22]. The technique is based on a Taylor series expansion of the discrete evolution equation. The atomistic system is considered for a large but fixed finite number N of atoms without passing to the limit $N \to \infty$. This is called the quasi-continuum regime. However, the resulting evolution model is often ill posed.

In this paper, we propose the so-called inner expansion technique for the upscaling from the atomic to the quasi-continuum level. It is based on a Taylor expansion of the deformation gradient. Just as in the direct expansion technique, it leads to a continuum mechanical potential such as (1.1) in which $\Phi^{(C),x}$ additionally depends on higher order derivatives of y. This allows us to capture the discreteness effects up to an arbitrary order. But in contrast to the direct expansion technique, well-posed evolution equations are obtained. Thus, our new technique avoids the disadvantages of both the scaling technique and the inner expansion technique.

Beyond the above-mentioned upscaling methods, many other techniques have

been developed. Without ambitions for completeness, let us note the work of Dreyer and Guckel [15], Friesecke and James [18], Friesecke and Matthies [19], Friesecke and Pego [20], and Friesecke and Theil [21]. Γ-limit techniques are studied by Braides and Gelli [8]. A further technique which transforms the original atomistic system to another discrete system with fewer degrees of freedom is given by the coarse-grained molecular dynamics technique [28]. Renormalization group methods have recently been investigated, e.g., in [11]. A classical reference for nonlinear lattice dynamics is the book by Born and Huang [7].

At first glance it seems useless to describe the discreteness effects by a continuum model, since the discrete atomistic model could be used directly instead. But this is not true. An advantage of the continuum model is that it is accessible to analytical techniques which allow us to further investigate its properties. For the numerical treatment, the continuum mechanical model will be discretized again. This way, i.e., via the continuum model and its successive discretization, the original discrete atomistic model is transformed into another discrete model. The key point here is that the mesh size can be arbitrarily chosen, in contrast to the fixed number of atoms in the original atomistic system. Thus, the discretization error can be controlled. Moreover, it can be balanced with the model error which depends on the degree of approximation used in the derivation of the respective continuum mechanical system. Altogether, the computational accuracy can thus be adjusted to the desired accuracy of the solution. This permits an efficient implementation and makes it possible to simulate larger systems. It even allows for adaptive techniques if necessary. In this respect the continuum model serves as an averaging tool to pass from the atomistic discretization size to an arbitrary discretization size.

This paper is organized as follows. First, the model on the atomic level is described in section 2. The classical scaling technique is reviewed and analyzed in section 3. In section 4, the direct expansion technique is shortly described, and it is shown how it preserves higher order effects which are lost by the scaling technique. We then come to our main result and present our inner expansion technique to derive a quasi-continuum model in section 5. It is discussed how this technique avoids the deficiencies of the direct expansion technique. Section 6 gives a numerical comparison of all three methods. Here we use the simple model problem of an atomic chain in the spirit of the famous work of Fermi, Pasta, and Ulam [17] to show the properties of the three different techniques and to discuss its differences. In section 7, the inner expansion technique is then applied to a realistic three-dimensional example, namely crystalline silicon. First, in section 7.1, the quality of the approximation of the continuum energy is analyzed in the stationary setting. This is done for a system of moderate size, which allows a direct comparison with the atomistic system. From this, the optimal order of approximation can be obtained for a reasonable error tolerance. The results are then used in section 7.2 to simulate the elastic behavior of the crystal for the corresponding evolution equation. The associated continuum system corresponds to an atomistic system of 12 billion atoms, which has been impossible to treat directly on the microscale with molecular dynamics techniques up to now.

2. Atomic level. On the atomic length scale, the specimen under consideration is described by a system of N interacting atoms. Its behavior is determined by the potential energy function $\Phi^{(A)}$, which depends on the atom positions $y_i \in \mathbb{R}^d$, $i = 1, \ldots, N$:

$$(2.1) \qquad \Phi^{(A)} = \Phi^{(A)}(\{y_i\}_{i=1,\ldots,N}).$$
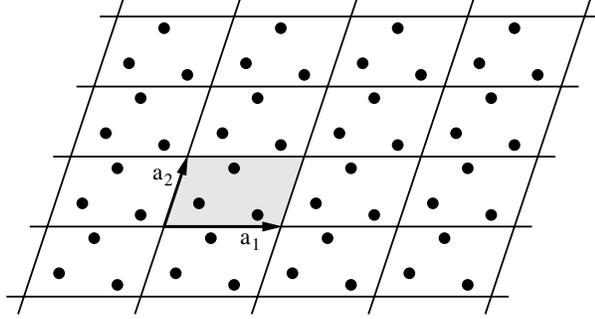
FIG. 1. *Two-dimensional example of a lattice $\mathcal{L}$ with its base cell and its spanning vectors.*

Here $d \in \mathbb{N}$ denotes the spatial dimension.

Now we choose a set of atom positions as the reference configuration in which the atoms are arranged in form of a lattice $\mathcal{L}$. Then the atom positions are given by

$$(2.2) \qquad \{y_i\}_{i=1,\ldots,N} = \mathcal{L} \cap \Omega,$$

where the domain $\Omega \subset \mathbb{R}^d$ describes the form of the crystal. Here the lattice $\mathcal{L}$ is the periodic infinite discrete set of atom positions

$$(2.3) \qquad \mathcal{L} := \{x + Az \mid x \in \mathcal{L}_{\text{cell}}, z \in \mathbb{Z}^d\},$$

where $A \in \mathrm{GL}(d, \mathbb{R})$ is a matrix. The base cell $\mathcal{L}_{\text{cell}} \subset \mathbb{R}^d$ is assumed to be nonempty and to consist of a small, finite number of atoms. In other words, $\mathcal{L}$ is the periodic continuation of $\mathcal{L}_{\text{cell}}$ along the parallelepiped which is spanned by the column vectors $a_1, a_2, \ldots, a_d \in \mathbb{R}^d$ of the matrix A. Figure 1 gives a two-dimensional example.

Now we assume that the crystal undergoes a deformation in space. This can be described by a function

$$(2.4) \qquad y : \mathcal{L} \cap \Omega \to \mathbb{R}^d,$$

which maps the reference configuration to the deformed state. A point $x \in \mathcal{L} \cap \Omega$ from the reference configuration is thus moved to $y(x)$ under deformation, and $y(\mathcal{L} \cap \Omega)$ describes the shape of the deformed crystal. The potential energy of the deformed crystal can now be written as

$$(2.5) \qquad \Phi^{(A)}(\{y(x)\}_{x \in \mathcal{L} \cap \Omega}).$$

Note that the positions of the atoms $\mathcal{L} \cap \Omega$ of the reference configuration act as an index set.

Furthermore, we assume that the potential can be split into a sum of local interactions $\Phi^{(A),\overline{x}}$ around some points $\overline{x}$:

$$(2.6) \qquad \Phi^{(A)}(\{y(x)\}_{x \in \mathcal{L} \cap \Omega}) = \sum_{\overline{x} \in \overline{\mathcal{L}} \cap \Omega} \Phi^{(A),\overline{x}}(\{y(x)\}_{x \in \mathcal{L} \cap \Omega}).$$

Almost all physically meaningful potentials allow such a localization. The points $\overline{x}$ can be interpreted as the center points of the local interactions. For example, $\overline{x}$ can be chosen as $\frac{1}{2}(x + \tilde{x})$ if $\Phi^{(A),\overline{x}}$ denotes the pair interaction of two atoms $y(x)$ and
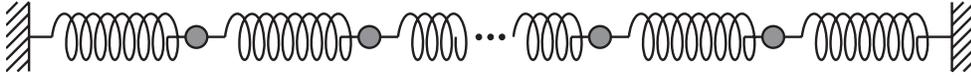
FIG. 2. *Atomic chain with springs and fixed boundary.*

$y(\tilde{x})$. The precise location of the points $\overline{x}$ will be relevant later for the inner expansion technique. For the other two techniques it suffices to treat the positions of the points $\overline{x}$ just as an index set. Thus we postpone their exact choice to section 5.3. Since the atom positions are arranged in the form of a lattice $\mathcal{L} \cap \Omega$, it makes sense to assume that this holds for the points $\overline{x}$ as well. The set of center points $\{\overline{x}\}$ then forms the associated lattice $\overline{\mathcal{L}} \cap \Omega$. Note that the lattice $\overline{\mathcal{L}}$ may, but need not, coincide with the original lattice $\mathcal{L}$.

Example 1. The most simple example is the atomic chain in one dimension. Despite its simplicity, it serves quite well as a model problem. Many effects from physically more complex situations can already be observed and studied with this model. We consider the domain $\Omega = (0, L)$ for some integer $L > 0$ and place the atoms at the points $1, 2, 3, \ldots, L - 2, L - 1$. The lattice is then given by $\mathcal{L} = \mathbb{Z}$. We assume that adjacent particles are connected by a spring of length one in the undeformed state. Furthermore, the chain is fixed at both ends; see Figure 2. The springs are assumed to obey Hooke's law with the spring constant normalized to one. This gives rise to the potential

(2.7)

$$\Phi^{(A)}(\{y(x)\}_{x \in \mathcal{L} \cap \Omega}) = \sum_{x=1}^{L} \varphi\big(y(x) - y(x-1)\big), \qquad \text{where} \qquad \varphi(r) = \frac{1}{2}(r-1)^2$$

for a deformation y. Here we assume $y(x) = x$ for all lattice points outside Ω, that is, for all $x \in \mathcal{L} \setminus \Omega$. This implements Dirichlet-like boundary conditions; i.e., the specimen is subjected to the identity deformation at its boundary. Note that these points outside Ω denote only "fixed particles" without any degree of freedom. They help to express the potential in a short form but do not constitute particles of the system.

We localize the potential by splitting it into the pair interactions. This leads to

(2.8)
$$\Phi^{(A)}(\{y(x)\}_{x \in \mathcal{L} \cap \Omega}) = \sum_{\overline{x} \in \overline{\mathcal{L}} \cap \Omega} \Phi^{(A),\overline{x}}(\{y(x)\}_{x \in \mathcal{L} \cap \Omega}),$$

where

(2.9)
$$\Phi^{(A),\overline{x}}(\{y(x)\}_{x \in \mathcal{L} \cap \Omega}) = \varphi\left(y\left(\overline{x} + \tfrac{1}{2}\right) - y\left(\overline{x} - \tfrac{1}{2}\right)\right)$$

with the associated lattice $\overline{\mathcal{L}} = \mathbb{Z} + \frac{1}{2}$.

Example 2. We now consider the well-known Lennard–Jones potential

(2.10)

$$\Phi^{(A)}(\{y(x)\}_{x \in \mathcal{L} \cap \Omega}) = \sum_{\substack{x, \tilde{x} \in \mathcal{L}, \ x < \tilde{x} \\ x \in \Omega \text{ or } \tilde{x} \in \Omega}} \varphi\big(y(x) - y(\tilde{x})\big), \quad \text{where} \quad \varphi(r) = \left(\frac{\sigma}{r}\right)^{12} - \left(\frac{\sigma}{r}\right)^{6}.$$

As in Example 1, the domain is given by $\Omega = (0, L)$, and the lattice is given by $\mathcal{L} = \mathbb{Z}$. Once more we assume $y(x) = x$ for all $x \in \mathcal{L} \setminus \Omega$ to prescribe Dirichlet-like boundary conditions. The side condition in the sum guarantees that each pair
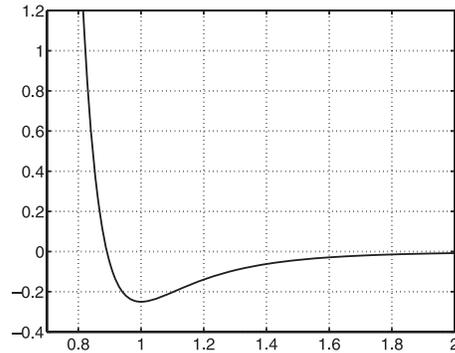
FIG. 3. *Function φ with $\sigma = 2^{-1/6}$ for the Lennard–Jones potential.*

of particles from the infinite lattice is accounted for exactly once if it contributes to $\Omega \cap \mathcal{L}$ at all. The choice of the associated lattice $\overline{\mathcal{L}} \cap \Omega$ and the according localization is not straightforward here. Therefore we postpone this issue to section 5, where it is systematically investigated.

The parameter $\sigma \in \mathbb{R}^+$ determines the lattice constant. The function φ possesses a sole minimum at $r = 2^{1/6}\sigma$ for positive arguments r; see Figure 3. For the choice $\sigma = 2^{-1/6}$ this minimum would be located at the lattice distance $r = 1$. Note, however, that this choice does not make the identity deformation $y(x) = x$ a minimizer of the potential energy of the system, since only adjacent particles are in the minimum of φ, whereas all other particle pairs (with larger distances) contribute to the potential energy by an attracting part. Therefore the minimum distance is a little bit smaller. We compensate for this by choosing σ slightly larger such that the minimum of the potential energy of the overall system is attained at $r = 1$. The corresponding parameter σ can be computed as follows: The potential energy of a particle in an infinite chain with lattice distance one is given by

$$(2.11) \qquad \frac{1}{2} \sum_{z \in \mathbb{Z} \backslash \{0\}} \varphi(z) = \sum_{z=1}^{\infty} \left[\left(\frac{\sigma}{z} \right)^{12} - \left(\frac{\sigma}{z} \right)^6 \right] = \zeta(12)\sigma^{12} - \zeta(6)\sigma^6,$$

where ζ denotes the Riemann ζ-function

$$(2.12) \qquad \zeta(s) = \sum_{z=1}^{\infty} \frac{1}{z^s}.$$

We require that the first derivative of (2.11) with respect to σ vanishes; hence we choose

$$(2.13) \qquad \sigma = \left(\frac{1}{2} \frac{\zeta(6)}{\zeta(12)} \right)^{\frac{1}{6}}.$$

The values $\zeta(6)$ and $\zeta(12)$ are given in Table 1. Since they are close to 1, the use of σ as in (2.13) is only a small modification to the previous choice $\sigma = 2^{-\frac{1}{6}}$.

Both the spring potential and the Lennard–Jones potential are pair potentials; i.e., they can be written as a sum of terms, each of which depends only on the positions of two atoms. This restriction, however, prevents the modeling of many physical properties. It can be shown, for example, that each pair potential exhibits the

TABLE 1
Values of the Riemann ζ-function.

s	$\zeta(s)$
6	1.017343061984449137145179279$\ldots$
12	1.000246086553308048298637998005$\ldots$

symmetry relation $C_{12} = C_{44}$ for the resulting elastic moduli, the so-called Cauchy relation [14]. Physical measurements of the elastic moduli of real solids, however, show that this symmetry is often not valid. Thus, pair potentials are not sufficient to model solids. Physically more meaningful potentials have been developed for several materials by Brenner [9], Stillinger and Weber [29], Abell [1], Tersoff [31], Daw and Baskes (embedded-atom method) [13, 14], and many others. They involve many-body interactions. Note that these potentials can also be localized as in (2.6) and are thus suitable for the methods described in the following.

3. Scaling technique. Now we are interested in deriving a macroscopic continuum mechanical model from a given atomistic system. A common method for this is the so-called scaling technique. It has been used and further analyzed by Blanc, Le Bris, and Lions [5], E and Huang [16], and many others.

3.1. Description of scheme. We consider a fixed domain $\Omega \subset \mathbb{R}^d$ and a fixed lattice $\mathcal{L}$ as in the previous section. Now we scale the lattice by some factor $\varepsilon \in \mathbb{R}^+$ and replace $\mathcal{L} \cap \Omega$ in (2.2) by $\varepsilon \mathcal{L} \cap \Omega$. For $\varepsilon < 1$, this corresponds to a description of the solid with more atoms. The original atomistic potential $\Phi^{(A)}$ and the local potentials $\Phi^{(A),\overline{x}}$ for $\overline{x} \in \overline{\mathcal{L}} \cap \Omega$ as defined in (2.6) are given on the length scale of the physical lattice constant. We denote this length scale by one. Now the original potentials cannot directly be applied to the length scale ε but must be rescaled properly. To this end, we multiply the arguments of $\Phi^{(A),\overline{x}}$ with ε^{-1}. If the points $\{y(x)\}_{x \in \varepsilon \mathcal{L} \cap \Omega}$ denote the atom positions on the length scale ε, then the points $\{\varepsilon^{-1} y(x)\}_{x \in \varepsilon \mathcal{L} \cap \Omega}$ are atom positions on the length scale one. They now can be used for the physical potential $\Phi^{(A),\overline{x}}$. This way, the potential $\Phi^{(A),\overline{x},\varepsilon}$ for the length scale ε is obtained from $\Phi^{(A),\overline{x}}$ by

$$(3.1) \qquad \Phi^{(A),\overline{x},\varepsilon}(\{y(x)\}_{x \in \varepsilon \mathcal{L} \cap \Omega}) := \Phi^{(A),\overline{x}}(\{\varepsilon^{-1} y(x)\}_{x \in \varepsilon \mathcal{L} \cap \Omega}).$$

The total potential $\Phi^{(A),\varepsilon}$ for the length scale ε is then given by the sum over $\Phi^{(A),\varepsilon,\overline{x}}$ for all atoms $\overline{x} \in \varepsilon \overline{\mathcal{L}} \cap \Omega$. Since the number $N_\varepsilon = |\varepsilon \overline{\mathcal{L}} \cap \Omega|$ of expansion points on the length scale ε scales such as ε^{-d}, i.e., $N_\varepsilon \approx \varepsilon^{-d} N_1$, we multiply this sum by ε^d to keep the total potential energy at the order $\mathcal{O}(1)$. Altogether, we obtain

$$\Phi^{(A),\varepsilon}(\{y(x)\}_{x \in \varepsilon \mathcal{L} \cap \Omega}) := \varepsilon^d \sum_{\overline{x} \in \varepsilon \overline{\mathcal{L}} \cap \Omega} \Phi^{(A),\varepsilon,\overline{x}}(\{y(x)\}_{x \in \varepsilon \mathcal{L} \cap \Omega})$$

$$(3.2) \qquad\qquad = \varepsilon^d \sum_{\overline{x} \in \varepsilon \overline{\mathcal{L}} \cap \Omega} \Phi^{(A),\overline{x}}(\{\varepsilon^{-1} y(x)\}_{x \in \varepsilon \mathcal{L} \cap \Omega}).$$

Note that $\Phi^{(A),\varepsilon,\overline{x}}$ acts here as a discrete energy density.

An equivalent way of constructing $\Phi^{(A),\varepsilon}$ is to replace the domain Ω by the scaled domain $\varepsilon^{-1}\Omega$, to fill it with atoms by means of $\mathcal{L} \cap \varepsilon^{-1}\Omega$, and then to define $\Phi^{(A),\varepsilon}$ as $\varepsilon^d \Phi^{(A)}$ on this set.

Now assume that the deformation y is not only given on the discrete sets $\mathcal{L} \cap \Omega$ or $\varepsilon \mathcal{L} \cap \Omega$ but continuously on the whole domain Ω, i.e., $y : \Omega \to \mathbb{R}^d$. Then the potential

energy of y can be defined for any length scale $\varepsilon > 0$ by restricting y to $\varepsilon \mathcal{L} \cap \Omega$, i.e.,

$$(3.3) \qquad \Phi^{(A),\varepsilon}(y) := \Phi^{(A),\varepsilon}(\{y(x)\}_{x \in \varepsilon \mathcal{L} \cap \Omega}).$$

Now the challenge is to determine the continuum limit

$$(3.4) \qquad \Phi^{(S)}(y) := \lim_{\varepsilon \to 0} \Phi^{(A),\varepsilon}(y).$$

The limit potential energy $\Phi^{(S)}$ is then used in a model on the macroscale.

For simple pair potentials which satisfy a certain decay condition that ensures finiteness of the sums, it can be shown that this limit is of the form (1.1); see [5] for a rigorous proof. We expect that similar results also hold for more complicated many-body potentials, though we are not aware of any proof in the literature. Note, however, that the mere existence of the limit does not yet say anything about its *quality*, i.e., which information from the microscale is kept on the macroscale and which is not. This point will be examined in more detail in the next section.

3.2. Typical examples. We now analyze how the scaling technique performs for typical sample problems. For the situation of Example 1, the following lemma holds according to [5, Theorem 1].

LEMMA 3.1. *Let $y \in C^2(\overline{\Omega})$. Then the continuum limit obtained from the scaling technique for the atomic chain with the spring potential* (2.7) *is given by*

$$(3.5) \qquad \Phi^{(S)}(y) = \lim_{\varepsilon \to 0} \Phi^{(A),\varepsilon}(y) = \int_{\Omega} \varphi(y'(x)) \, \mathrm{d}x.$$

For the proof, the difference $y(\overline{x} + \frac{1}{2}) - y(\overline{x} - \frac{1}{2})$ for some point $\overline{x} \in \overline{\mathcal{L}} \cap \Omega$ is transformed under the scaling procedure to the difference quotient

$$(3.6) \qquad \frac{y(\overline{x} + \varepsilon\frac{1}{2}) - y(\overline{x} - \varepsilon\frac{1}{2})}{\varepsilon},$$

which nicely converges to $y'(\overline{x})$. Furthermore, the sum $\varepsilon \sum_{\overline{x} \in \overline{\varepsilon}\mathcal{L} \cap \Omega}$ is a Riemann sum for the integral. The smoothness assumption on y then allows us to simultaneously perform both limit processes.

Similarly, the scaling technique works fine for nonlocal interactions as given in Example 2. Again [5, Theorem 1] provides us with the following lemma.

LEMMA 3.2. *Let $y \in C^2(\overline{\Omega})$. Then the continuum limit obtained from the scaling technique for the atomic chain with the Lennard–Jones potential* (2.10) *is given by*

$$(3.7) \qquad \Phi^{(S)}(y) = \lim_{\varepsilon \to 0} \Phi^{(A),\varepsilon}(y) = \frac{1}{2} \int_{\Omega} \sum_{z \in \mathbb{Z} \setminus \{0\}} \varphi(y'(x)z) \, \mathrm{d}x.$$

Here the infinite sum can be explicitly determined. It holds that

$$\frac{1}{2} \sum_{z \in \mathbb{Z} \setminus \{0\}} \varphi(y'(x)z) = \sum_{z=1}^{\infty} \left[\left(\frac{\sigma}{y'(x)z} \right)^{12} - \left(\frac{\sigma}{y'(x)z} \right)^{6} \right]$$

$$(3.8) \qquad = \left(\frac{\sigma}{y'(x)} \right)^{12} \zeta(12) - \left(\frac{\sigma}{y'(x)} \right)^{6} \zeta(6) = \overline{\varphi}(y'(x)),$$

where

$$(3.9) \qquad \overline{\varphi}(r) = \zeta(12) \left(\frac{\sigma}{r} \right)^{12} - \zeta(6) \left(\frac{\sigma}{r} \right)^{6}.$$

Hence the continuum energy (3.7) reads as

$$\Phi^{(S)}(y) = \int_\Omega \overline{\varphi}(y'(x)) \, \mathrm{d}x. \tag{3.10}$$

The function $\overline{\varphi}$ plays the role of an "effective Lennard–Jones potential." It is close to φ since $\zeta(6)$ and $\zeta(12)$ are close to 1. This resembles the fact that the far-field interactions contribute to the overall potential only up to a small extent due to the rapid decay of the Lennard–Jones potential.

Both the spring potential and the Lennard–Jones potential are relatively simple potentials. Physically meaningful potentials of real solids are much more complex. As already described above, it is often not sufficient to deal with pair potentials only; instead one has to take into account many-body interactions as well. This, however, can have adverse effects for the scaling technique, as will be seen from the next (still simple) example of a three-body potential.

Example 3. Again we consider the atomic chain. Let $\mathcal{L} = \overline{\mathcal{L}} = \mathbb{Z}$, and replace the spring potential of Example 1 by the following three-body interaction potential:

$$\Phi^{(A)}(y) = \sum_{\overline{x} \in \overline{\mathcal{L}} \cap \Omega} \varphi\big(y(\overline{x} + 1) - 2y(\overline{x}) + y(\overline{x} - 1)\big). \tag{3.11}$$

Here φ can be any continuous function. We then have the following lemma.

LEMMA 3.3. *Let $\Omega \subset \mathbb{R}$ be a bounded domain. Let $y \in C^2(\overline{\Omega})$, and let φ be continuous at 0. Then the continuum limit obtained from the scaling technique for the atomic chain with potential* (3.11) *is given by*

$$\Phi^{(S)}(y) = \int_\Omega \varphi(0) \, \mathrm{d}x. \tag{3.12}$$

Proof. The scaled potential is given by

$$\Phi^{(A),\varepsilon}(y) = \varepsilon \sum_{\overline{x} \in \varepsilon \overline{\mathcal{L}} \cap \Omega} \varphi\left(\frac{y(\overline{x} + \varepsilon) - 2y(\overline{x}) + y(\overline{x} - \varepsilon)}{\varepsilon} \right). \tag{3.13}$$

The Taylor expansion of $y(\overline{x} + \varepsilon)$ and $y(\overline{x} - \varepsilon)$ around $\overline{x}$ gives

$$\varphi\left(\frac{y(\overline{x} + \varepsilon) - 2y(\overline{x}) + y(\overline{x} - \varepsilon)}{\varepsilon} \right) = \varphi\left(\varepsilon y''(\xi_{\overline{x}})\right) \tag{3.14}$$

for some point $\xi_{\overline{x}} \in \Omega$. Now let $\mathrm{vol}\,\Omega := \int_\Omega 1 \, \mathrm{d}x$ denote the volume of Ω, and let card denote the cardinality of a set. We then obtain

(3.15)

$$\left| \Phi^{(A),\varepsilon}(y) - \int_\Omega \varphi(0) \, \mathrm{d}x \right|$$

$$= \left| \varepsilon \sum_{\overline{x} \in \varepsilon \overline{\mathcal{L}} \cap \Omega} \Big(\varphi\big(\varepsilon y''(\xi_{\overline{x}})\big) - \varphi(0) \Big) - \varphi(0) \big(\mathrm{vol}\,\Omega - \varepsilon \,\mathrm{card}(\varepsilon\overline{\mathcal{L}} \cap \Omega)\big) \right|$$

$$\leq \varepsilon \,\mathrm{card}(\varepsilon\overline{\mathcal{L}} \cap \Omega) \max_{\overline{x} \in \varepsilon\overline{\mathcal{L}} \cap \Omega} \left| \varphi\big(\varepsilon y''(\xi_{\overline{x}})\big) - \varphi(0) \right| + |\varphi(0)| \big|\mathrm{vol}\,\Omega - \varepsilon \,\mathrm{card}(\varepsilon\overline{\mathcal{L}} \cap \Omega)\big|$$

$$\overset{\varepsilon \to 0}{\longrightarrow} 0$$

since y'' is bounded and $\varepsilon \,\mathrm{card}(\varepsilon\overline{\mathcal{L}} \cap \Omega) \to \mathrm{vol}\,\Omega$ as $\varepsilon \to 0$. $\quad\square$

Hence $\Phi^{(S)}$ is a constant functional and gives no information about the system at all.

The continuum limit obtained by the scaling technique is completely useless for this specific model problem. We admit that the interaction potential (3.11) is somewhat artificial and marks an extreme case. However, this example shows an effect which can occur for the scaling technique if many-body potentials are used instead of pair potentials.

The reason for this failure of the scaling technique will be examined in the following section.

3.3. Asymptotic analysis. Consider the Taylor series expansion of the deformation function y around a point $\hat{x} \in \Omega$. Without loss of generality we set $\hat{x} = 0$, and the same behavior for general $\hat{x} \in \Omega$ is obtained after a translation. If we assume for the moment that the series expansion exists and converges to y, we obtain

$$
\begin{aligned}
\Phi^{(A),\varepsilon,0}(\{y(x)\}_{x\in\varepsilon\mathcal{L}\cap\Omega}) &= \Phi^{(A),\varepsilon,0}\left(\left\{\sum_{k=0}^{\infty}\frac{1}{k!}x^k y^{(k)}(0)\right\}_{x\in\varepsilon\mathcal{L}\cap\Omega}\right) \\
&= \Phi^{(A),0}\left(\left\{\varepsilon^{-1}\sum_{k=0}^{\infty}\frac{1}{k!}(\varepsilon x)^k y^{(k)}(0)\right\}_{x\in\mathcal{L}\cap\varepsilon^{-1}\Omega}\right) \\
&= \Phi^{(A),0}\left(\left\{\sum_{k=0}^{\infty}\varepsilon^{k-1}\frac{1}{k!}x^k y^{(k)}(0)\right\}_{x\in\mathcal{L}\cap\varepsilon^{-1}\Omega}\right).
\end{aligned}
$$

(3.16)

The terms with $k = 0$ would blow up to infinity as $\varepsilon \to 0$. However, since every physically reasonable potential is translation-invariant, these terms do not appear at all. The terms with $k = 1$ are of order one. They are thus captured by the limit process, and the first derivatives show up in the limit continuum energy. All higher terms, i.e., those with $k \geq 2$, disappear in the limit process because $\varepsilon^{k-1} \to 0$ as $\varepsilon \to 0$.

Therefore the continuum energy obtained by the scaling technique depends only on the first derivatives. The scaling preserves the terms of the first nonvanishing order $k = 1$. All higher order effects of the potential are lost by this type of scaling and the limiting process. This is just what happened in Example 3, where the arguments of the potential function formed a difference stencil for the second derivative.

4. Direct expansion technique. To preserve the higher order effects which are lost by the scaling technique as described in the previous section, the so-called direct expansion technique can be used. It has been proposed by Kruskal and Zabusky [23], Zabusky and Kruskal [37], Collins [10], and Rosenau [24, 25, 26] and is based on the Taylor expansion of the evolution equation of the atomistic system. This approach leads to a quasi-continuum description, i.e., a continuum mechanical model for the atomistic system for a fixed number N of atoms. The limiting process $N \to \infty$ is omitted, and thus the discreteness of the atomistic system is not destroyed. The potential itself is not treated directly, but it is possible to reconstruct the continuum potential afterwards.

The method will now be shortly described for the atomic chain with the spring potential (2.7); for further details see [24]. According to Newton's second law of motion, the evolution reads as

$$
(4.1) \qquad m\frac{\partial^2}{\partial t^2}y(x) = \varphi'\big(y(x+1) - y(x)\big) - \varphi'\big(y(x) - y(x-1)\big) \qquad \forall x \in \mathcal{L} \cap \Omega,
$$

where m denotes the mass of each atom. In terms of the discrete lattice width $z(x) := y(x) - y(x-1)$, it can be written as

$$(4.2) \qquad m\frac{\partial^2}{\partial t^2}z(x) = \varphi'(z(x+1)) - 2\varphi'(z(x)) + \varphi'(z(x-1)).$$

Taylor expansion of $\varphi' \circ z$ around x leads to

$$(4.3) \qquad m\frac{\partial^2}{\partial t^2}z(x) = L(\varphi' \circ z)(x)$$

with the infinite series of differential operators

$$(4.4) \qquad L = 4\sinh^2\left(\frac{1}{2}\frac{\partial}{\partial x}\right) = \sum_{k=1}^{\infty}\frac{2}{(2k)!}\frac{\partial^{2k}}{\partial x^{2k}} = \frac{\partial^2}{\partial x^2} + \frac{1}{12}\frac{\partial^4}{\partial x^4} + \frac{1}{360}\frac{\partial^6}{\partial x^6} + \dots;$$

L is then truncated at the desired order.

For a chain of linear springs, i.e., $\varphi(r) = \frac{1}{2}(r-1)^2$ as in Example 1, and a truncation of L after the fourth derivative, this leads to

$$(4.5) \qquad m\frac{\partial^2}{\partial t^2}z(x) = \frac{\partial^2}{\partial x^2}z(x) + \frac{1}{12}\frac{\partial^4}{\partial x^4}z(x).$$

Now the quasi-continuum potential energy $\Phi^{(\mathrm{D})}$ can be reconstructed. For this purpose, we have to find a potential function from which the evolution equation results by computing the directional derivative and applying the discrete formula of partial integration. This leads to

$$(4.6) \qquad \Phi^{(\mathrm{D})}(z) = \sum_{x \in \mathcal{L} \cap \Omega}\frac{1}{2}z'^2(x) - \frac{1}{24}z''^2(x).$$

Note that the atomistic evolution equation is rewritten in terms of the variable z in this approach. Thus the resulting equations are expressed in terms of the changed variable z, which plays the role of the deformation gradient: $z \approx \partial y/\partial x$. Hence (4.5) does not correspond to an evolution equation for y but to an evolution equation for its first spatial derivative.

In the example considered here, the simple pair potential depends on the difference $y(x) - y(x-1)$. Thus the change of variables from $y(x)$ to $z(x) = y(x) - y(x-1)$ allowed us to express the potential and its derivative in terms of a single variable, which then led to the formulations (4.5) and (4.6). In principle, any translation invariant N-body potential can be written in terms of the differences of $N-1$ pairs of atom position. Thus, this approach should work for many-body potentials as well. However, the corresponding equations can then become quite involved.

Furthermore, note that the coefficients of the series L of differential operators depend on the number of atoms. To analyze this dependence, the evolution equation (4.1) is scaled as in section 3:

$$(4.7)$$
$$\varepsilon m\frac{\partial^2}{\partial t^2}y(x) = \varphi'\left(\frac{y(x+\varepsilon) - y(x)}{\varepsilon}\right) - \varphi'\left(\frac{y(x) - y(x-\varepsilon)}{\varepsilon}\right) \qquad \forall x \in \varepsilon\mathcal{L} \cap \Omega.$$

Here the mass of the atoms scales with ε to keep the total mass of the system constant. The difference equation is then rewritten in terms of the normalized lattice width $z(x) := \frac{y(x)-y(x-\varepsilon)}{\varepsilon}$ as

$$(4.8) \qquad m\frac{\partial^2}{\partial t^2}z(x) = \frac{\varphi'(z(x+\varepsilon)) - 2\varphi'(z(x)) + \varphi'(z(x-\varepsilon))}{\varepsilon^2}.$$

Then the Taylor expansion of $\varphi' \circ z$ leads to (4.3) with the differential operator

$$(4.9) \qquad L = \sum_{k=1}^{\infty}\frac{2}{(2k)!}\varepsilon^{2k-2}\frac{\partial^{2k}}{\partial x^{2k}} = \frac{\partial^2}{\partial x^2} + \frac{\varepsilon^2}{12}\frac{\partial^4}{\partial x^4} + \frac{\varepsilon^4}{360}\frac{\partial^6}{\partial x^6} + \cdots.$$

Clearly, the principal part $\partial^2/\partial x^2$ remains unaffected by the scaling, but the higher order terms, i.e., the dispersion effects, are weighted by certain polynomials in ε. Their influence now depends on the specific choice of ε and is substantially reduced for $\varepsilon < 1$. They would completely vanish in the limit $\varepsilon \to 0$, which is consistent with the results of the scaling technique.

Let us note a major drawback of the direct expansion technique: The evolution equation (4.5) is ill posed, since the right-hand side is not a negative semidefinite operator in space. In other words, the equation lacks hyperbolicity. As a consequence, the potential energy dramatically blows up during the time evolution. This leads to an uncontrolled behavior of the solution if the corresponding evolution equation can be solved at all. Contrary to this, the evolution equation of the original atomistic model is well posed. The upscaling process by the direct expansion technique therefore must have destroyed essential properties of the atomistic model. A closer look at the continuum potential energy (4.6) shows that it is not bounded from below, although this holds for the original atomistic potential (2.7). Furthermore, the continuum potential is not convex, in contrast to its atomistic counterpart. Thus the direct expansion technique does not preserve these two important properties. This leads to the nonhyperbolicity of (4.5) and makes it ill posed.

Note that if the differential operator L is truncated after the sixth-order term, the resulting evolution equation is well posed by chance. We conclude from these observations that an arbitrary truncation of L is sometimes feasible but that it does not lead in general to a well-posed evolution equation.

Several ways to overcome this problem have been proposed. If (4.5) would be replaced by

$$(4.10) \qquad m\frac{\partial^2}{\partial t^2}z(x) = \frac{\partial^2}{\partial x^2}z - \frac{1}{12}\frac{\partial^4}{\partial x^4}z,$$

i.e., if the sign of the fourth-order term would be altered, then the equation would be well posed. This is known as the wrong sign problem, and (4.5) is denoted as the bad Boussinesq equation; see [24]. Another way to overcome this problem is to replace the Taylor series expansion of L by a more general Padé approximation; see, e.g., [36] and [25, 26]. Sometimes these approximations lead to a well-posed evolution equation, but sometimes they do not. Thus, these approaches also do not satisfactorily correct the problems of the direct expansion technique.

5. Inner expansion technique. To remedy the disadvantages of the scaling technique and the direct expansion technique as described in sections 3 and 4, respectively, we propose a so-called inner expansion technique. This approach gives a

description of the atomistic system within the quasi-continuum regime. It captures all higher order terms up to a given order, conserves convexity, and leads to well-posed evolution equations.

5.1. Inner expansion. In (2.6) we introduced the points $\overline{x} \in \overline{\mathcal{L}} \cap \Omega$ to localize the overall potential energy $\Phi^{(A)}$ by means of the sum $\sum_{\overline{x} \in \overline{\mathcal{L}} \cap \Omega} \Phi^{(A),\overline{x}}$. For each point $\overline{x}$, we now consider the Taylor series expansion of the deformation function y around $\overline{x}$ up to some degree $K \in \mathbb{N}$:

$$(5.1) \qquad y(x) \approx \sum_{k=0}^{K} \frac{1}{k!} \nabla^k y(\overline{x}) : (x - \overline{x})^k.$$

Here the colon denotes the higher-dimensional scalar product. The expansion (5.1) then allows us to reformulate the local potential $\Phi^{(A),\overline{x}}$ from (2.6) in the following way:

$$\Phi^{(A),\overline{x}}(\{y(x)\}_{x \in \mathcal{L} \cap \Omega}) \approx \Phi^{(A),\overline{x}} \left(\left\{ \sum_{k=0}^{K} \frac{1}{k!} \nabla^k y(\overline{x}) : (x - \overline{x})^k \right\}_{x \in \mathcal{L} \cap \Omega} \right)$$

$$(5.2) \qquad\qquad = \Phi^{(I),\overline{x}}\left(y(\overline{x}), \nabla y(\overline{x}), \nabla^2 y(\overline{x}), \dots, \nabla^K y(\overline{x}) \right),$$

where $\Phi^{(I),\overline{x}}$ is defined by

$$(5.3) \qquad \Phi^{(I),\overline{x}}(d^0, d^1, d^2, \dots, d^K) := \Phi^{(A),\overline{x}} \left(\left\{ \sum_{k=0}^{K} \frac{1}{k!} d^k : (x - \overline{x})^k \right\}_{x \in \mathcal{L} \cap \Omega} \right).$$

Thus we transformed the original potential $\Phi^{(A),\overline{x}}$ which depends on the deformation y at all lattice points $x \in \mathcal{L} \cap \Omega$ to a representation which depends on the derivatives of y only at the single point $\overline{x}$. Note the similarity of this construction to expansion (3.16) in section 3.3.

Summing up the local potentials $\Phi^{(I),\overline{x}}$, we obtain the overall potential

$$(5.4) \qquad \Phi^{(I)}(y) = \sum_{\overline{x} \in \overline{\mathcal{L}} \cap \Omega} \Phi^{(I),\overline{x}}\left(y(\overline{x}), \nabla y(\overline{x}), \nabla^2 y(\overline{x}), \dots, \nabla^K y(\overline{x}) \right).$$

5.2. Spatial averaging. The potential energy $\Phi^{(I)}$ in representation (5.4) still contains the finite sum over all expansion points $\overline{x} \in \overline{\mathcal{L}} \cap \Omega$. This is in contrast to common continuum mechanical energies in which an energy density is integrated over the reference configuration Ω. The sum will now be approximated as follows: Observe that (5.4) is a Riemann sum which is close to an integral. This justifies it to interpolate $\Phi^{(I)}(y)$ by passing to the integral representation

$$(5.5) \qquad \Phi^{(J)}(y) = \frac{1}{|\det A|} \int_{\Omega} \Phi^{(I),\overline{x}}\left(y(\overline{x}), \nabla y(\overline{x}), \nabla^2 y(\overline{x}), \dots, \nabla^K y(\overline{x}) \right) \, \mathrm{d}\overline{x}.$$

The factor $\frac{1}{|\det A|}$ stems from the volume of the base cell of the lattice; cf. (2.3).

Here the following remark is in order: The scaling technique is based on the thermodynamic limit, which drives the number N of atoms to infinity. In this case the limiting procedure $N \to \infty$ includes the limit of the Riemann sum, and an integral representation is directly obtained. In contrast to this approach, the number N of atoms is kept fixed for both the direct expansion technique and the inner expansion

technique. The passage from the Riemann sum to the integral representation (5.5) is now an additional approximation step which does not correspond to the process of letting the number N of atoms tend to infinity. The result is not a description for the continuum limit but an interpolated description for the system with a fixed number of atoms in the quasi-continuum regime, which still contains the discreteness effects of the finite system.

5.3. Choice of expansion points. Now we consider the choice of the expansion points $\overline{x}$ in more detail. In order to make the truncated Taylor series approximation as accurate as possible, the remainder terms must be minimized. The latter strongly depend on the choice of the expansion points; hence it is crucial to choose them correctly.

The optimal choice can be given strictly in the important special case when the local potential $\Phi^{(A),\overline{x}}$ depends on a linear combination of all components of all points $y(x)$. This means that the local potential can be written as

$$(5.6) \qquad \Phi^{(A),\overline{x}}(\{y(x)\}_{x \in \mathcal{L} \cap \Omega}) = \varphi\left(\sum_{x \in \mathcal{L} \cap \Omega} a_x \cdot y(x)\right),$$

where $\varphi : \mathbb{R} \to \mathbb{R}$ is a function and $a_x \in \mathbb{R}^d$ are constants for all $x \in \mathcal{L} \cap \Omega$. For the sake of a simple description, we proceed with $d = 1$. Similar arguments hold for higher space dimensions. Because of the crystal symmetry, we can assume that the absolute values of the coefficients a_x satisfy the symmetry relation

$$(5.7) \qquad |a_x| = |a_{2c-x}|$$

for a center point $c \in \Omega$ such that $\mathcal{L} = 2c - \mathcal{L}$. Then

$$
\begin{aligned}
\sum_{x \in \mathcal{L} \cap \Omega} |a_x| x &= \frac{1}{2} \sum_{x \in \mathcal{L} \cap \Omega} |a_x| x + |a_{2c-x}|(2c - x) \\
(5.8) \qquad &= \frac{1}{2} \sum_{x \in \mathcal{L} \cap \Omega} |a_x| x + |a_x|(2c - x) = \sum_{x \in \mathcal{L} \cap \Omega} |a_x| c.
\end{aligned}
$$

Thus the center point c can equivalently be characterized as the barycenter

$$(5.9) \qquad c = \frac{\sum_{x \in \mathcal{L} \cap \Omega} |a_x| x}{\sum_{x \in \mathcal{L} \cap \Omega} |a_x|}.$$

The Taylor expansion of the potential $\Phi^{(A),\overline{x}}$ from (5.6) around $\overline{x}$ then reads as

$$
\begin{aligned}
\varphi\left(\sum_{x \in \mathcal{L} \cap \Omega} a_x y(x)\right) = \varphi\bigg(&\sum_{x \in \mathcal{L} \cap \Omega} \sum_{k=0}^{K} \frac{a_x}{k!} y^{(k)}(\overline{x})(x - \overline{x})^k \\
(5.10) \qquad &+ \frac{a_x}{(K+1)!} y^{(K+1)}(\xi_x)(x - \overline{x})^{K+1}\bigg)
\end{aligned}
$$

for some points $\xi_x \in \Omega$. Since a priori nothing is known about the behavior of $y^{(K+1)}$, the best way is to minimize the simplified remainder term

$$(5.11) \qquad R(\overline{x}) := \sum_{x \in \mathcal{L} \cap \Omega} |a_x| |x - \overline{x}|^{K+1}.$$

LEMMA 5.1. *The simplified remainder term* (5.11) *attains its minimum at the barycenter c.*

Proof. Since the function $\overline{x} \mapsto |x - \overline{x}|^{K+1}$ is convex, we can bound $R(\overline{x})$ from below by

$$R(\overline{x}) \geq \sum_{x \in \mathcal{L} \cap \Omega} |a_x| \left(\left.\frac{\partial |x - \overline{x}|^{K+1}}{\partial \overline{x}}\right|_{\overline{x}=c} (\overline{x} - c) + |x - c|^{K+1} \right)$$

$$(5.12) \qquad = \sum_{x \in \mathcal{L} \cap \Omega} |a_x||x - c|^{K+1} = R(c).$$

Here, due to symmetry, the relation $\left.\frac{\partial |x-\overline{x}|^{K+1}}{\partial \overline{x}}\right|_{\overline{x}=c} = -\left.\frac{\partial |2c-x-\overline{x}|^{K+1}}{\partial \overline{x}}\right|_{\overline{x}=c}$ holds, and the differential terms $\frac{\partial |x-\overline{x}|^{K+1}}{\partial \overline{x}}$ disappear in the above sum. □

Hence each point $\overline{x}$ should be chosen as the barycenter c of the local interaction potential. The set $\overline{\mathcal{L}} \cap \Omega$ is thus constructed by splitting the overall potential $\Phi^{(A)}$ into as many local interactions as possible. For each local interaction the barycenter c is computed according to (5.9), and its value is assigned to the variable $\overline{x}$. The set of all such barycenters c then forms the set $\overline{\mathcal{L}} \cap \Omega$.

In the case of a more general potential which cannot be written as (5.6), many remainder terms occur and are combined in a complex manner. Their interaction can be very complicated and depends strongly on the type of the potential. It is unclear what the minimization of the remainder terms in this case means. An individual analysis is necessary for each such type of potential. Furthermore, the barycenter c of the local interaction cannot be strictly defined due to the missing coefficients a_x. Nevertheless, in many cases it is possible to define some generalized barycenter. From our experience it is best to choose $\overline{x}$ as such a center point.

5.4. Examples. We now apply the inner expansion technique to the already introduced sample problems. First, we consider the atomic chain with the spring potential (2.7) as given by Example 1. The barycenter for the interaction of the particles $y(x)$ and $y(x + 1)$ is given by $x + \frac{1}{2}$; hence the expansion points as given by (2.9) already fit to this scheme. We apply our inner expansion method and obtain from a straightforward calculation the following lemma.

LEMMA 5.2. *Let $K \in \mathbb{N}$ denote the order of approximation, and let $y \in C^K(\overline{\Omega})$. Then the quasi-continuum energy density obtained from the inner expansion technique for the atomic chain with the spring potential* (2.7) *is given by*

$$(5.13) \qquad \Phi^{(I),\overline{x}}(d^0, \ldots, d^K) = \varphi\left(\sum_{\substack{k=1 \\ k \text{ odd}}}^{K} \frac{1}{k!2^{k-1}} d^k \right).$$

Thus, for $K = 1$ and $K = 2$ we end up with the interpolated quasi-continuum energy

$$(5.14) \qquad \Phi^{(J)}(y) = \frac{1}{2} \int_\Omega (y'(x) - 1)^2 \, \mathrm{d}x.$$

Note that it coincides with the outcome of the scaling technique and the direct expansion technique with truncation after the second-order term. Larger parameters K result in additional discreteness terms. We obtain

$$(5.15) \qquad \Phi^{(J)}(y) = \frac{1}{2} \int_\Omega \left(y'(x) + \frac{1}{24} y'''(x) - 1 \right)^2 \, \mathrm{d}x$$

for $K = 3$ and $K = 4$ and

$$(5.16) \qquad \Phi^{(J)}(y) = \frac{1}{2} \int_\Omega \left(y'(x) + \frac{1}{24} y'''(x) + \frac{1}{1920} y'''''(x) - 1 \right)^2 \, dx$$

for $K = 5$ and $K = 6$.

Now we are interested in how the inner expansion technique performs in cases where the scaling technique fails. To this end, we again consider the atomic chain with the three-body potential (3.11) from Example 3. For this case we have the following lemma.

LEMMA 5.3. *Let $K \in \mathbb{N}$ denote the order of approximation, and let $y \in C^K(\overline{\Omega})$. Then the quasi-continuum potential energy density obtained from the inner expansion technique for the atomic chain with the potential* (3.11) *is given by*

$$(5.17) \qquad \Phi^{(I),\overline{x}}(y) = \varphi \left(\sum_{\substack{k=1 \\ k \text{ even}}}^K \frac{2}{k!} y^{(k)}(\overline{x}) \right).$$

For $K = 2$ and $K = 3$ this results in the potential energy

$$(5.18) \qquad \Phi^{(J)}(y) = \int_\Omega \varphi\left(y''(\overline{x})\right) \, d\overline{x},$$

and for $K = 4$ and $K = 5$ the potential energy

$$(5.19) \qquad \Phi^{(J)}(y) = \int_\Omega \varphi\left(y''(\overline{x}) + \frac{1}{12} y''''(\overline{x}) \right) \, d\overline{x}$$

is obtained. We see that the expansion technique yields a meaningful continuum energy also for the case where the scaling technique failed.

The inner expansion technique is certainly not limited to the case of quadratic potentials and to local interactions. We demonstrate this for the Lennard–Jones potential from Example 2. According to Lemma 5.1, we choose the barycenter $\overline{x} = \frac{1}{2}(x + \tilde{x})$ for each term of the sum (2.10). This leads to $\overline{\mathcal{L}} = \frac{1}{2}\mathbb{Z} \cap \Omega$. To circumvent an annoying formalism with the boundary, we treat all atoms to be contained in an infinite bulk crystal. This is reasonable due to the rapid decay of the Lennard–Jones potential. The atomistic potential is localized by

$$(5.20)$$

$$\Phi^{(A),\overline{x}}(\{y(x)\}_{x \in \mathcal{L} \cap \Omega}) = \begin{cases} \displaystyle\sum_{z=1}^\infty \varphi\big(y(\overline{x} + z) - y(\overline{x} - z)\big) & \text{if } \overline{x} \in \mathbb{Z} \cap \Omega, \\ \displaystyle\sum_{z=1}^\infty \varphi\big(y(\overline{x} + z - \tfrac{1}{2}) - y(\overline{x} - z + \tfrac{1}{2})\big) & \text{if } \overline{x} \in (\mathbb{Z} + \tfrac{1}{2}) \cap \Omega; \end{cases}$$

cf. also (2.6).

Then we substitute the Taylor series expansion (5.1) of y into (5.20) and reformulate the potential according to (5.2). This leads to the following lemma.

LEMMA 5.4. *Let $K \in \mathbb{N}$ denote the order of approximation, and let $y \in C^K(\overline{\Omega})$. Then the interpolated quasi-continuum energy obtained from the inner expansion tech-*

nique for the atomic chain with the Lennard–Jones potential (2.10) *is given by*

(5.21)

$$\Phi^{(J)}(y) = \int_\Omega \sum_{z=1}^\infty \varphi \left(\sum_{\substack{k=1 \\ k \text{ odd}}}^K \frac{2}{k!} y^{(k)}(\overline{x}) z^k \right) + \sum_{z=1}^\infty \varphi \left(\sum_{\substack{k=1 \\ k \text{ odd}}}^K \frac{2}{k!} y^{(k)}(\overline{x}) \left(z - \frac{1}{2} \right)^k \right).$$

For $K = 1$ and $K = 2$, this results in

(5.22)
$$\Phi^{(J)}(y) = \int_\Omega \overline{\varphi}(y'(\overline{x})) \, d\overline{x},$$

where $\overline{\varphi}$ is given by (3.9). This expression coincides with the continuum limit by the scaling technique. For $K = 3$ and $K = 4$, we obtain

(5.23)
$$\Phi^{(J)}(y) = \int_\Omega \sum_{z=1}^\infty \varphi \left(y'(\overline{x})z + \frac{1}{24} y'''(\overline{x})z^3 \right) \, d\overline{x}.$$

For $K \geq 3$, no closed form is known to us which avoids the sum over all z as in (5.22). Again we see that in comparison to the scaling technique now higher order terms are generated by the inner expansion technique.

6. Comparison of upscaling schemes. After the discussion of three different methods to derive a continuum or quasi-continuum description of an atomistic model, the question arises of how the corresponding continuum models and their solutions differ or coincide. To this end, we numerically solve the corresponding evolution equations and compare the results. Here the solution of the original atomistic system serves as a reference solution. Furthermore, we show that convexity of the atomistic model is preserved under the scaling technique and the inner expansion technique, which leads to well-posed macroscopic evolution equations.

6.1. Comparison of evolution equations. For the atomistic system, the evolution equation is given by Newton's second law of motion, which states that the force acting on each atom equals its mass times its acceleration. The force points towards the direction of steepest descent of the potential energy, that is, its negative gradient with respect to the coordinates of the respective atom. In the case of a continuum potential of the form

(6.1)
$$\Phi^{(C)}(y) = \int_\Omega \Phi^{(C),x} \left(y(x), \nabla y(x), \ldots, \nabla^K y(x) \right) \, dx$$

as it is derived by the scaling technique, the direct expansion technique, and the inner expansion technique, this generalizes to

(6.2)
$$\int_\Omega \rho \frac{\partial^2 y}{\partial t^2} v \, dx = -\Phi^{(C)'}(y; v)$$

for all test functions $v \in C_c^\infty(\Omega)$. Here $\rho = |\det A|^{-1} m$ denotes the mass density, and $\Phi^{(C)'}(y; v)$ denotes the derivative of $\Phi^{(C)}$ at y in the direction v. We compute

$$\Phi^{(C)'}(y; v) = \int_\Omega \sum_{k=0}^K \Phi_{,k}^{(C),x}(y, \nabla y, \ldots, \nabla^K y) : \nabla^k v \, dx$$

(6.3)
$$= \int_\Omega \sum_{k=0}^K (-1)^k \operatorname{div}^k \Phi_{,k}^{(C),x}(y, \nabla y, \ldots, \nabla^K y) v \, dx,$$

where $\Phi_{,k}^{(\mathrm{C}),x}$ denotes the derivative of $\Phi^{(\mathrm{C}),x}$ with respect to the argument $\nabla^k y$. Since this holds for any test function $v \in C_c^\infty(\Omega)$, the macroscopic evolution PDE reads as

$$(6.4) \qquad \rho \frac{\partial^2 y}{\partial t^2} = \sum_{k=0}^{K} (-1)^{k+1} \, \mathrm{div}^k \, \Phi_{,k}^{(\mathrm{C}),x}(y, \nabla y, \nabla^2 y, \dots, \nabla^K y) \qquad \text{in } \Omega.$$

It has to be equipped with the initial values

$$(6.5) \qquad y(x,0) = y_0(x) \quad \text{and} \quad \frac{\partial y}{\partial t}(x,0) = y_1(x) \qquad \forall x \in \Omega$$

and with the Dirichlet-like boundary conditions

(6.6)
$$y(x,t) = x, \quad \nabla_\nu y(x,t) = \nu, \quad \nabla_\nu^2 y(x,t) = \dots = \nabla_\nu^{K-1} y(x,t) = 0 \quad \forall x \in \partial\Omega, t > 0.$$

The latter stem from the fixation of the specimen at its boundary. To this end, we embed the specimen in an infinite undeformed crystal. This implies for the continuum model that y and its normal derivatives coincide with the identity deformation and its normal derivatives at the boundary.

Now we discretize the evolution equation (6.4) in time and space by finite differences. For the time discretization, an explicit Euler scheme with a three-point stencil is sufficient. For the spatial discretization, we exploit the divergence structure of the PDE by a two-stage scheme. In the first step, the derivatives $\Phi_{,k}^{(\mathrm{C}),x}$ are computed. In the second step, the divergence operators are applied. In both steps, a difference stencil of sufficiently high consistency order is necessary to resolve the spatial derivatives. A stencil which is consistent only up to order one or two would introduce higher order error terms. These would interfere with the higher order derivatives of the continuum model which resemble the discreteness of the atomistic system. Since we are interested in the discreteness effects of the PDE and not in the consistency error of the finite difference discretization, we have to use stencils with sufficiently high order. Therefore, in all numerical examples given below, eight-point stencils are applied in both steps. Their consistency order is eight minus the order of the respective derivative. In all applications studied below, this results in a discretization error of at least order four due to the two-stage scheme and a maximal order of eight of the considered PDEs. Thus the spatial discretization errors of low order are eliminated, and dispersion comes basically from the higher order terms of the PDE itself and not from the finite difference discretization.[2]

In the following we study the behavior of the numerical solutions of the macroscopic evolution equations obtained from the scaling technique and the inner expansion technique. The direct expansion technique with the truncation of L after the fourth-order term is not considered because the corresponding evolution equation is ill posed. We use the atomistic potentials given in Examples 1–3 from sections 2 and 3.

The domain is chosen as $\Omega = (0, 1000)$. This corresponds to a chain of 999 atoms with lattice constant one. The initial values at time $t = 0$ are given by $y(x,0) = x + p(x)$ and by $\frac{\partial y}{\partial t}(x,0) = 0$ for all $x \in \Omega$. Here the function introduces a small

---

[2]To guarantee that roundoff errors do not destroy the high order of the respective scheme, a mantissa size of 512 bits has been used for the numerical calculations.

TABLE 2
Spatial error and convergence rates for the solution of (6.7) *at* $t = 400$.

Spatial res.	Error	Ratio	$\log_2(\text{ratio})$
1000	4.167261e-02		
2000	5.864973e-03	7.105359	2.828903
4000	3.535252e-05	165.899726	7.374168
8000	1.489190e-07	237.394333	7.891142
16000	5.900347e-10	252.390197	7.979512
32000	2.302158e-12	256.296296	8.001769

TABLE 3
Spatial error and convergence rates for the solution of (6.8) *at* $t = 20$.

Spatial res.	Error	Ratio	$\log_2(\text{ratio})$
500	8.962375e-02		
1000	1.081729e-02	8.285232	3.050542
2000	1.328105e-04	81.449043	6.347826
4000	8.599413e-06	15.444137	3.948987
8000	1.646067e-07	52.242194	5.707143

smooth perturbation around the center point $x = 500$. To be precise, p is a piecewise 21th-order polynomial such that $p \equiv 0$ on $[0, 490] \cup [510, 1000]$, $p(500) = 1$ and $p'(x) = p''(x) = \cdots = p^{(10)}(x) = 0$ for $x = 490, 500, 510$.

The Dirichlet conditions (6.6) on the left and on the right boundary are implemented by additional ghost points outside of Ω whose values are kept fixed to the identity deformation. This leads to a consistency order of one only. But since we later consider sufficiently short time intervals such that the evolution of the initial perturbation will not reach the boundary, this low consistency order at the boundary is ineffective and will not destroy the high consistency order of the differential operator in the interior of the domain. Of course, if one is interested in calculating the long-term behavior of solutions which includes boundary interactions, more involved techniques must be used to really retain the high consistency order of the interior also at the boundary and to simultaneously guarantee the stability of the discretization at the boundary; see, e.g., [6].

First, we study the spring potential from Example 1. The mass is normalized to one. For the inner expansion technique with $K = 1$ and $K = 2$, the scaling technique, and the direct expansion technique with a truncation of L at the second-order term, the resulting evolution equations all coincide and read as

$$(6.7) \qquad \frac{\partial^2 y}{\partial t^2} = \frac{\partial^2 y}{\partial x^2}.$$

For the inner expansion technique with $K = 3$ and $K = 4$ the resulting evolution equation is given by

$$(6.8) \qquad \frac{\partial^2 y}{\partial t^2} = \frac{\partial^2 y}{\partial x^2} + \frac{1}{12} \frac{\partial^4 y}{\partial x^4} + \frac{1}{576} \frac{\partial^6 y}{\partial x^6}.$$

We now numerically solve the discretized equations as described above. The convergence behavior of the spatial discretization is depicted in Tables 2 and 3. Here the error was measured in the maximum norm. To this end, the numerical solution with a spatial resolution of 64,000 and 16,000 for (6.7) and (6.8), respectively, was
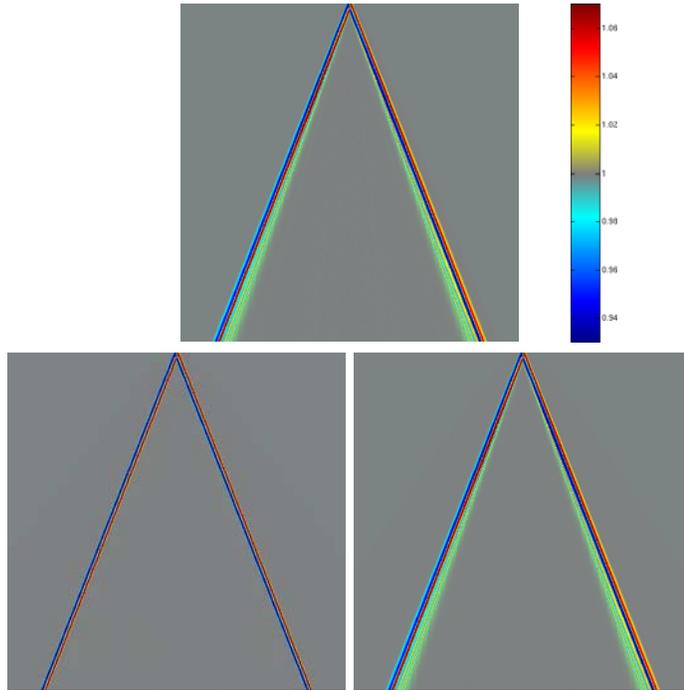
FIG. 4. *Example* 1: *Solutions of the particle system (top),* (6.7) *(lower left), and* (6.8) *(lower right).*

used as reference. We used a time step of $\delta t = 0.01$ and $\delta t = 0.001$ for the solution of (6.7) and (6.8), respectively. From Table 2 we see that the expected convergence order eight[3] is fully reached for model (6.7). For model (6.8) we roughly obtain the expected order six.

The time evolution of the numerically computed solutions of (6.7) and (6.8) is shown in Figure 4. To this end, the x-axis is plotted horizontally, and the t-axis is plotted vertically going from top to bottom. Moreover, the color indicates the quantity $(y')^{-1}$, which corresponds to the atom density of the atomistic model. Grey denotes the equilibrium, whereas yellow and red denote regions with a high particle density and blue denotes regions with a low particle density; cf. also the color bar in Figure 4 (top right). The time evolution of the solution of the original particle system is given in Figure 4 (top left) for reference.

In all cases, we can clearly observe the propagation of the initial perturbation with constant speed to the left and to the right side. The propagation speed is correctly reproduced for both continuum models. For the model (6.7), the initial perturbation is propagated without changing its shape. This is in full agreement with the established theory for the linear wave equation (6.7). However, this behavior does not match that of the original atomistic system. Here a distinct amount of dispersion due to the discreteness of the underlying atomistic system can be observed. The absence of the dispersion is immanent to the scaling technique, because it describes the thermodynamic limit $N \to \infty$ and not the quasi-continuum behavior for a large

---

[3]The stencil guarantees a convergence order of at least seven. Due to symmetry the order increases by one here.

TABLE 4
Error of solution of the quasi-continuum model obtained by the direct expansion technique for Example 1 *at* $t = 400$ *with respect to solution of original particle system.*

K	2-norm of error	∞-norm of error
1	1.9306179105e-1	7.2139674139e-2
3	1.0595174636e-2	3.0471826890e-3
5	4.3215088073e-3	9.2014282448e-4

but finite N. In the limit the dispersion vanishes; cf. (4.9). This dispersion, however, is captured by the continuum model for $K = 3, 4$. Its solution coincides very well with the solution of the original atomistic system. The dispersion is reproduced both qualitatively and quantitatively to a high extent.

We also tested the inner expansion technique for $K \geq 5$, which leads to quasi-continuum models involving additional terms with higher derivatives than those in (6.8). The resulting solutions (of course we then used finite difference stencils of appropriate higher order) differ only slightly from those of (6.8). The difference is not noticeable in a plot such as in Figure 4. The corresponding error with respect to the solution of the original particle system is given in Table 4. Here we see that the error is approximately 20 times smaller for $K = 3$ than for $K = 1$ but only two times smaller for $K = 5$ than for $K = 3$. Thus, the expansion technique with $K = 3$ already gives a very good quasi-continuum approximation of the model. The involved terms up to the sixth-order derivative suffice to accurately describe the microscopic effects.

Now we turn to the Lennard–Jones potential of Example 2. We use the same atomic chain with 999 atoms as in Example 1. The time step is chosen as $\delta t = 0.01$. The main difference from the previous example is the nonlinearity of the evolution equation. Thus we have to deal with shocks. The initial configuration is the same as in Example 1, the only difference being that we have chosen a wider support (400) of the perturbation function p to make the shocks more visible.

The time evolution of the numerically computed solutions of the original atomistic system and of the macroscopic models obtained by the inner expansion technique with $K = 1$ and $K = 3$ are shown in Figure 5. For $K = 1$, the evolution equation again coincides with the outcome of the scaling technique and of the direct expansion technique with truncation at order two. We can observe essentially the same propagation of the initial perturbation towards both boundaries as in Example 1. Note that now the propagation speed is no longer constant due to the nonlinearity; i.e., the perturbation changes its shape. After a certain time, sharp shock waves develop, which can clearly be seen in all solutions. Furthermore, note that in the vicinity of the shock waves the solution of the original atomistic model shows a distinct scattering. This dispersive effect is disturbed on the macroscopic level for $K = 1$, but it is captured to a very high extent for $K = 3$; see the enlarged parts of the respective solutions in Figure 6.

Finally, we address Example 3. Again we use the same setting as for Example 1. Only the atomistic potential is replaced by (3.11) with $\varphi(r) = \frac{1}{2}r^2$. For this atomistic potential, the scaling technique failed. Therefore we compare only the inner expansion technique for $K = 2$ and $K = 4$. The macroscopic evolution equations are given by

$$(6.9) \qquad\qquad \frac{\partial^2 y}{\partial t^2} = -\frac{\partial^4 y}{\partial x^4} \qquad \text{for } K = 2, 3$$
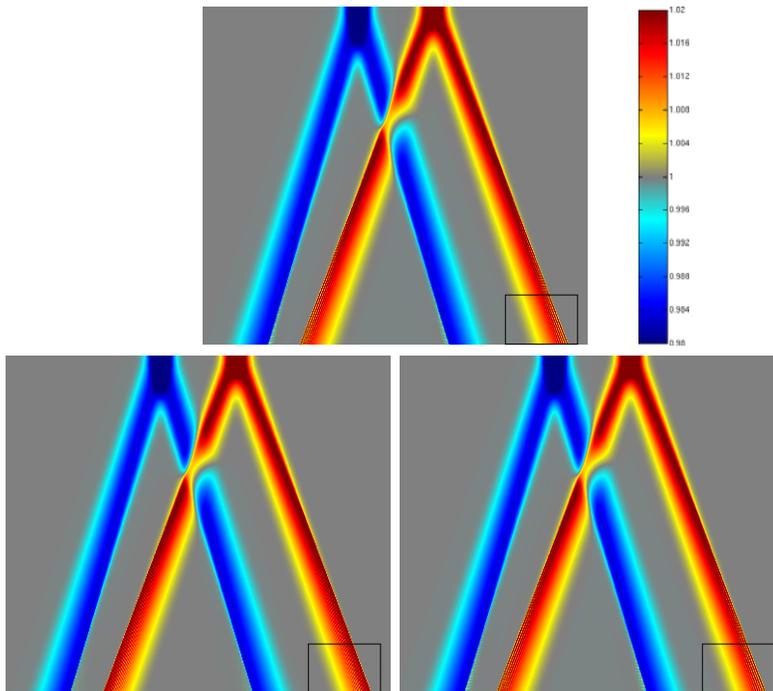
FIG. 5. *Example* 2: *Solutions of the particle system (top) and quasi-continuum system for* $K = 1$ *(lower left) and* $K = 3$ *(lower right). The indicated regions are enlarged in Figure 6.*
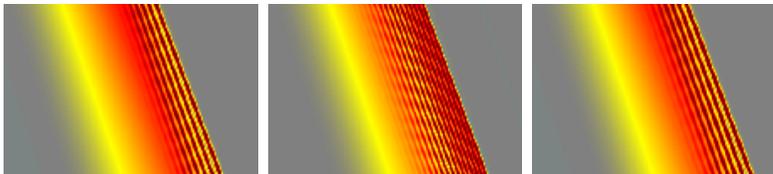
FIG. 6. *Example* 2: *Zoomed regions from Figure* 5: *the particle system (left) and quasi-continuum system for* $K = 1$ *(center) and* $K = 3$ *(right).*

and

$$(6.10) \qquad \frac{\partial^2 y}{\partial t^2} = -\frac{\partial^4 y}{\partial x^4} - \frac{1}{6}\frac{\partial^6 y}{\partial x^6} - \frac{1}{144}\frac{\partial^8 y}{\partial x^8} \qquad \text{for } K = 4, 5,$$

respectively.

The time evolution of the numerically computed solutions of the original atomistic system and of (6.9) and (6.10) are shown in Figure 7. All three solutions are in good agreement. The fanning out pattern is captured qualitatively very well. However, a closer look reveals that the angles of the resulting striped delta shapes are not correctly reproduced for $K = 2$. But for $K = 4$, they are very close to the ones of the particle system. The width of the solution pattern at the last time step which determines this angle is indicated in Figure 7. It measures about 725 particles for the particle system, 900 particles for the continuum system with $K = 2$, and 750 particles for $K = 4$.
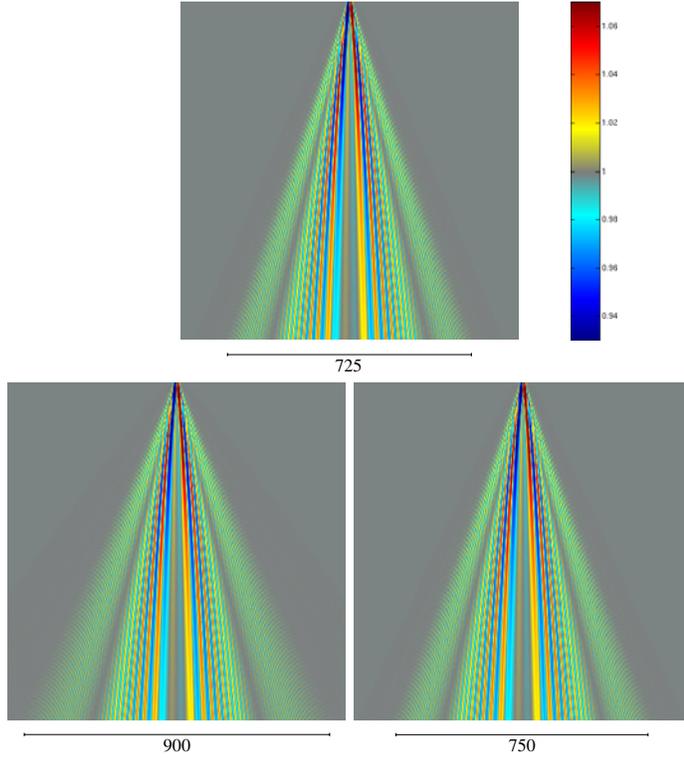
FIG. 7. *Example* 3: *Solutions of the particle system (top),* (6.9) *(lower left), and* (6.10) *(right).*

The evolution equation (4.5) governed by the direct expansion technique is not included in our comparison, because it is ill posed and cannot be solved, as already mentioned in section 4. We nevertheless tried to solve it numerically. This attempt failed as expected. The solution behaved chaotically and exploded after a few time steps. In the next section, we show that this cannot happen to continuum models which are obtained by the scaling technique or our new inner expansion technique.

6.2. Hyperbolicity. The essential criterion for whether the evolution equations studied here are well posed or ill posed is hyperbolicity. We call (6.4) hyperbolic if the right-hand side is a negative semidefinite operator in space. This property holds if the continuum potential is convex. Now, if the original atomistic potential already is not convex, this cannot be expected to hold for the resulting continuum potential. But if the original atomistic potential is convex, it still depends on the upscaling scheme whether or not this property is carried over to the continuum level. Therefore it is important to investigate which upscaling techniques preserve convexity and which do not.

We already discussed in section 4 that the direct expansion technique in general does not retain the convexity of the atomistic potential. Consequently, the right-hand side of the corresponding evolution equation (4.5) needs not to be a negative semidefinite operator, and the resulting macroscopic equation can be ill posed. This problem is avoided by the scaling technique and the inner expansion technique. In contrast to the direct expansion technique, they both retain the convexity of the

atomistic potential. One immediately obtains from the description of the respective schemes the following lemma.

LEMMA 6.1. *Let the atomistic potential* $\Phi^{(A)}$ *be convex. Then the continuum potentials* $\Phi^{(I)}$, $\Phi^{(J)}$, *and* $\Phi^{(S)}$ *are convex as well.*

As a consequence, the corresponding macroscopic evolution equations are hyperbolic and well posed.

LEMMA 6.2. *Assume that the continuum potential* (6.1) *is convex. Then the corresponding evolution equation* (6.3) *is hyperbolic.*

Proof. It has to be verified that the spatial operator of (6.3) is negative semidefinite. To this end, we test with $y - \mathrm{id}$. By the mean value theorem we have for some intermediate function $\tilde{y} = \mathrm{id} + \vartheta(y - \mathrm{id})$ with $\vartheta \in (0,1)$:

$$
-\int_\Omega \sum_{k=0}^K (-1)^k \operatorname{div}^k \Phi_{,k}^{(C),x}(y, \nabla y, \ldots, \nabla^K y)(y - \mathrm{id}) \, \mathrm{d}x
$$

$$
= -\int_\Omega \sum_{k=0}^K \Phi_{,k}^{(C),x}(y, \nabla y, \ldots, \nabla^K y) : \nabla^k (y - \mathrm{id}) \, \mathrm{d}x
$$

$$
= -\int_\Omega \sum_{k=0}^K \Phi_{,k}^{(C),x}(\mathrm{id}, I, 0, \ldots, 0) : \nabla^k (y - \mathrm{id}) \, \mathrm{d}x
$$

$$
\quad - \int_\Omega \sum_{k,l=0}^K \nabla^l (y - \mathrm{id}) : \Phi_{,k,l}^{(C),x}(\tilde{y}, \nabla \tilde{y}, \ldots, \nabla^K \tilde{y}) : \nabla^k (y - \mathrm{id}) \, \mathrm{d}x
$$

(6.11) $\qquad = -\Phi^{(C)\prime}(\mathrm{id}; y - \mathrm{id}) - \Phi^{(C)\prime\prime}(\tilde{y}; y - \mathrm{id}, y - \mathrm{id}).$

Here the boundary integrals which arise from the partial integration vanish due to the boundary conditions. The first directional derivative $\Phi^{(C)\prime}(\mathrm{id}; y - \mathrm{id})$ vanishes because id is an equilibrium configuration. The second directional derivative $\Phi^{(C)\prime\prime}(\tilde{y}; y - \mathrm{id}, y - \mathrm{id})$ is nonnegative, since the potential $\Phi^{(C)}$ is assumed to be convex. Hence the expression (6.11) is nonpositive. $\square$

Note that the Lennard–Jones potential is locally convex around the equilibrium configuration but not globally convex. However, if the initial conditions are close to the equilibrium, then the solution is close to the equilibrium as well. Thus, if the initial conditions are chosen sufficiently small, the solution stays within this convex region. Then the locally convex potential acts as a globally convex potential, and the above argumentation works for this case as well.

7. Application to silicon. So far, we introduced the inner expansion technique, studied it for a simple one-dimensional model problem, and compared it to the scaling technique and the direct expansion technique. The inner expansion technique proved to be a useful technique to obtain a quasi-continuum description of the atomistic system, which avoids the drawbacks of the other methods. We now apply it to an atomistic model of crystalline silicon to see whether its advantages hold for this more realistic problem in three dimensions as well.

7.1. Approximation of potential energy. A widely used potential for the atomistic simulation of silicon is given by Stillinger and Weber [29]. It consists of

two- and three-body interactions and reads as

$$(7.1) \quad \Phi^{(A)}(\{y(x)\}_{x \in \mathcal{L} \cap \Omega}) = \frac{1}{2} \sum_{x_1,x_2} \varphi_2(|y(x_2) - y(x_1)|)$$

$$+ \frac{1}{2} \sum_{x_1,x_2,x_3} \varphi_3\left(|y(x_2) - y(x_1)|, |y(x_3) - y(x_1)|, \frac{(y(x_2) - y(x_1)) \cdot (y(x_3) - y(x_1))}{|y(x_2) - y(x_1)||y(x_3) - y(x_1)|}\right).$$

Here the summation is over all $x_1, x_2, x_3 \in \mathcal{L} \cap \Omega$ with $x_1 \neq x_2 \neq x_3 \neq x_1$. The two- and three-body terms are given by

$$(7.2) \qquad\qquad \varphi_2(r) = \varepsilon A \left(B \frac{\sigma^4}{r^4} - 1\right) \exp \frac{\sigma}{r - \sigma b},$$

$$(7.3) \qquad \varphi_3(r_{12}, r_{13}, \Theta) = \varepsilon \lambda \exp\left(\frac{\gamma\sigma}{r_{12} - \sigma b} + \frac{\gamma\sigma}{r_{13} - \sigma b}\right)\left(\Theta + \frac{1}{3}\right)^2.$$

For both types of interactions, the exponential terms serve as smooth cutoff functions, which make the potential local. The pair interaction φ_2 attains its minimum for the nearest neighbor distance in the lattice and therefore stabilizes the equilibrium distance of two adjacent atoms in the lattice. The variable Θ denotes the cosine of the angle between $y(x_2) - y(x_1)$ and $y(x_3) - y(x_1)$. The triple term attains its minimum for the angle $\arccos\left(-\frac{1}{3}\right) \approx 109.47°$. The involved constants are

$$(7.4) \qquad \begin{aligned} & A = 7.049556277, \quad \lambda = 21.0, \sigma = 0.20951 \text{ nm}, \ b = 1.8, \\ & B = 0.6022245584, \gamma = 1.2, \quad \varepsilon = 50 \text{ kcal/mol}. \end{aligned}$$

Together the pair and triple interactions result in an overall potential which is minimal just if the atoms are arranged in the so-called diamond structure. This is the natural lattice structure of silicon. It consists of two nested fcc lattices. With the notation of (2.3), it can be written as

$$(7.5) \qquad \mathcal{L}_{\text{cell}} = \frac{a_0}{4} \left\{ \begin{pmatrix} 0 \\ 0 \\ 0 \end{pmatrix}, \begin{pmatrix} 2 \\ 2 \\ 0 \end{pmatrix}, \begin{pmatrix} 0 \\ 2 \\ 1 \end{pmatrix}, \begin{pmatrix} 2 \\ 0 \\ 1 \end{pmatrix}, \begin{pmatrix} 1 \\ 1 \\ 2 \end{pmatrix}, \begin{pmatrix} 3 \\ 3 \\ 2 \end{pmatrix}, \begin{pmatrix} 1 \\ 3 \\ 3 \end{pmatrix}, \begin{pmatrix} 3 \\ 1 \\ 3 \end{pmatrix} \right\}$$

and $A = a_0 I$, where I denotes the 3×3 unit matrix and $a_0 = 0.54309$ nm denotes the lattice constant. Figure 8 shows a part of the lattice. Here pairs of nearest neighbor atoms are connected by bonds.

We now apply the inner expansion technique in a straightforward but tedious calculation to the potential of Stillinger and Weber. To this end, the overall potential $\Phi^{(A)}$ from (7.1) is split into all two-body and three-body interactions. The expansion points $\bar{x}$ are chosen as $\bar{x} = \frac{1}{2}(x_1 + x_2)$ for the two-body terms and as $\bar{x} = \frac{1}{3}(x_1 + x_2 + x_3)$ for the three-body terms. The Taylor series expansion with $K = 3$ of the term $y(x_2) - y(x_1)$ then reads as

$$y(x_2) - y(x_1) \approx (x_2 - x_1) \cdot \nabla y(\bar{x}) + \frac{1}{2}\left((x_2 - \bar{x})^2 - (x_1 - \bar{x})^2\right) : \nabla^2 y(\bar{x})$$

$$(7.6) \qquad\qquad\qquad + \frac{1}{6}\left((x_2 - \bar{x})^3 - (x_1 - \bar{x})^3\right) : \nabla^3 y(\bar{x}).$$

For $y(x_3) - y(x_1)$ we obtain an analogous expression. We now substitute $z_2 := x_2 - x_1$ and $z_3 := x_3 - x_1$ to pass over to difference vectors. This way the expansion (7.6) is
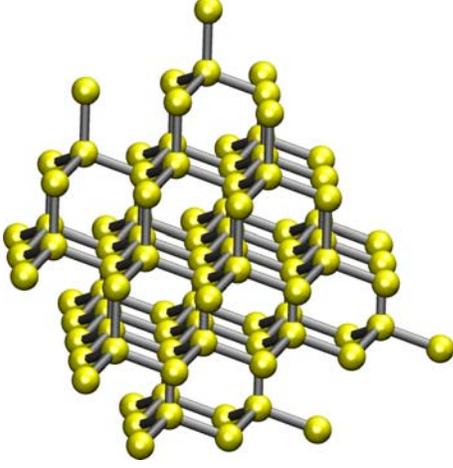
FIG. 8. *Diamond structure of a silicon crystal.*
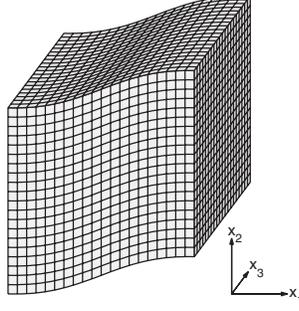
FIG. 9. *Deformation (7.12) for $\delta = 0.2$.*

transformed to

$$(7.7) \qquad T_{z_2}^1 := z_2 \cdot \nabla y(\overline{x}) + \frac{1}{6 \cdot 2^2} z_2{}^3 : \nabla^3 y(\overline{x})$$

for the two-body terms and to

$$T_{z_2,z_3}^2 := z_2 \cdot \nabla y(\overline{x}) + \frac{1}{18} \left((2z_2 - z_3)^2 - (z_2 + z_3)^2 \right) : \nabla^2 y(\overline{x})$$
$$+ \frac{1}{162} \left((2z_2 - z_3)^3 + (z_2 + z_3)^3 \right) : \nabla^3 y(\overline{x}),$$
$$T_{z_2,z_3}^3 := z_3 \cdot \nabla y(\overline{x}) + \frac{1}{18} \left((2z_3 - z_2)^2 - (z_2 + z_3)^2 \right) : \nabla^2 y(\overline{x})$$
$$(7.8) \qquad + \frac{1}{162} \left((2z_3 - z_2)^3 + (z_2 + z_3)^3 \right) : \nabla^3 y(\overline{x})$$

for the three-body terms. These expressions are substituted into the atomistic potential. We eliminate the boundary effects by replacing the sums $\sum_{z_2,z_3 \in \mathcal{L} \cap \Omega - x_1}$ by the sums $\sum_{z_2,z_3 \in \mathcal{L}}$ over the full lattice. This leads to the continuum energy density

$$(7.9) \quad \Phi^{(\mathrm{I}),\overline{x}}(\nabla y, \nabla^2 y, \nabla^3 y)$$
$$= \sum_{z_2 \in \mathcal{L}} \varphi_2 \left(\left| T_{z_2}^1 \right| \right) + \frac{1}{2} \sum_{z_2,z_3 \in \mathcal{L}} \varphi_3 \left(\left| T_{z_2,z_3}^2 \right|, \left| T_{z_2,z_3}^3 \right|, \frac{T_{z_2,z_3}^2 \cdot T_{z_2,z_3}^3}{\left| T_{z_2,z_3}^2 \right| \left| T_{z_2,z_3}^3 \right|} \right)$$

and the interpolated potential

$$(7.10) \qquad \Phi^{(\mathrm{J})}(y) = \frac{1}{a_0{}^3} \int_{\Omega} \Phi^{(\mathrm{I}),\overline{x}}(\nabla y, \nabla^2 y, \nabla^3 y) \, d\overline{x}.$$

The corresponding evolution equation is then given by

$$(7.11) \qquad a_0{}^3 \rho \frac{\partial^2 y}{\partial t^2} = \operatorname{div} \frac{\partial \Phi^{(\mathrm{I}),\bar{x}}}{\partial \nabla y} - \operatorname{div}^2 \frac{\partial \Phi^{(\mathrm{I}),\bar{x}}}{\partial \nabla^2 y} + \operatorname{div}^3 \frac{\partial \Phi^{(\mathrm{I}),\bar{x}}}{\partial \nabla^3 y} \qquad \text{in } \Omega.$$

To analyze how the quasi-continuum potential deviates from the original atomistic potential, we compute the potential energy on both the atomic level and the continuum mechanical level for the same system. We choose an atomistic system of 32768 atoms, where the atoms are arranged in the form of the diamond lattice and which is formed like a cube in the reference configuration. The system is embedded in a larger system of fixed atoms to constitute the Dirichlet-like boundary conditions as in the previous sections.

To obtain a nontrivial setting, the two opposite faces of the cube perpendicular to the x_1-axis are displaced by a shearing with a ratio δ ranging from 0 to 0.2. In between, the deformation of the specimen is smoothly interpolated by

$$(7.12) \qquad q(x_1, x_2, x_3) = (x_1, x_2 + \delta p(x_1), x_3).$$

Here p denotes the fifth-order polynomial such that $p(0) = 0$, $p(L) = \delta$, and $p'(0) = p''(0) = p'(L) = p''(L) = 0$, where L is the length of the cube edges. The deformation is shown in Figure 9 for $\delta = 0.2$.

Now the atomistic and the quasi-continuum potential for $K = 1, 2, 3$ is computed for each parameter δ. This is done separately for the two-body and three-body interactions. For the numerical quadrature of the integral in the quasi-continuum potential (5.5), a simple trapezoid rule with the cell size equivalent to one atomic cell is used. Of course, more sophisticated quadrature schemes with larger cell sizes could be employed for higher computational efficiency. But here the simple scheme corresponds directly to the finite sum (5.4) and does not introduce an integration error. This allows us to precisely evaluate the approximation quality of the expansion scheme and separate it from any integration error.

Hence we obtain values $\Phi_{B,\delta}^{(\mathrm{A})}$, $\Phi_{B,\delta,K}^{(\mathrm{I})}$ for $K = 1, 2, 3$, $\delta = 0, \dots, 0.2$, and $B = 2, 3$, where $B = 2$ denotes the two-body interactions and $B = 3$ the three-body interactions. In Figure 10, the absolute errors

$$(7.13) \qquad \Phi_{B,\delta,K}^{(\mathrm{I})} - \Phi_{B,\delta}^{(\mathrm{A})}$$

are displayed. One can clearly see that the approximation for $K = 3$ is much better than for $K = 1$ and $K = 2$. Furthermore, note that the curves for $K = 1$ and $K = 2$ coincide for the two-body potential. This is because the choice of the expansion point $\bar{x}$ as barycenter completely inhibits the dependency on the second derivative $\nabla^2 y$. Figure 10 also shows the relative error

$$(7.14) \qquad \frac{\Phi_{B,\delta,K}^{(\mathrm{I})} - \Phi_{B,\delta}^{(\mathrm{A})}}{\Phi_{B,\delta}^{(\mathrm{A})} - \Phi_{B,0}^{(\mathrm{A})}}.$$

For $K = 1$ and $K = 2$, it is below 0.07% and 0.3%, respectively. For $K = 3$, it is even below 0.003% and 0.004%. Especially the three-body angle terms profit from an approximation order of $K = 3$, because bending effects are captured correctly then, while they are in part lost for $K \leq 2$.

Thus it seems reasonable to use an approximation order of $K = 3$ for the Stillinger–Weber potential. Note, however, that the influence of the higher order contributions depends on the size of the system. This influence gets successively
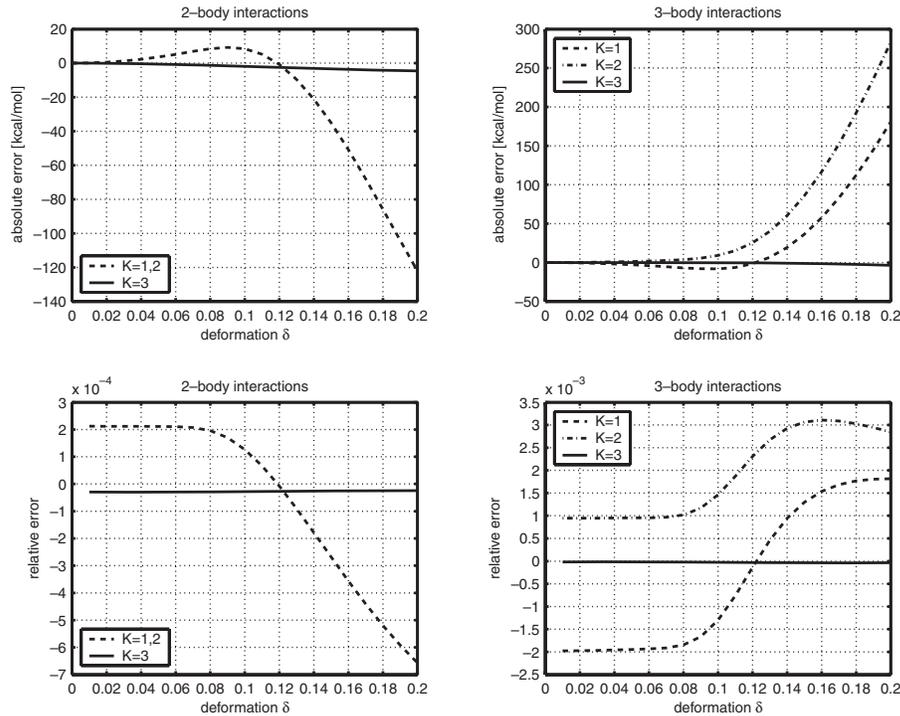
FIG. 10. *Absolute (top) and relative (bottom) errors of the Stillinger–Weber potential for the inner expansion technique. Left: two-body interactions* (7.2), *right: three-body interactions* (7.3).

smaller for an increasing number of atoms. For systems with a very high number of atoms, it can even be appropriate to use $K = 1$, since the higher order contributions are then negligibly small. But these contributions result in a qualitatively different behavior in the evolution equation as we have already seen in section 6.1. Thus it is justified to incorporate them despite their quantitatively small contribution to the overall energy.

7.2. Dynamics of elastic response. Now we consider the time evolution of a silicon crystal. According to the considerations in the previous subsection, we use the approximation order $K = 3$. The evolution is then governed by (7.11). We are interested in the elastic response of the crystal. To this end, we choose as initial value the deformation q as given by (7.12) with the deformation ratio $\delta = 0.1$, together with an initial velocity of zero. The boundary values are chosen in such a way that the specimen in embedded in an infinite bulk crystal which underwent the same deformation. Analogously to (6.6), this reads as

$$(7.15) \quad y(x,t) = q(x), \quad \nabla_\nu y(x,t) = \nabla_\nu q(x), \quad \nabla_\nu^2 y(x,t) = \nabla_\nu^2 q(x) \quad \forall x \in \partial\Omega, t > 0.$$

The spatial discretization is done by finite differences where we again exploit the divergence structure of the PDE as in the last section. This is even more important in the three-dimensional setting, since it considerably reduces the computational costs. In a first step, the discrete derivatives up to order three are computed. Then, in a second step, the discrete divergence operators are applied. For both steps, a difference stencil formed as the tensor product of one-dimensional five-point stencils is used. The

stencils are consistent of order four for the first and second derivative and of order two for the third derivative. This ensures a sufficient accuracy. For the time discretization, an explicit Euler scheme is applied.

The dimensions are chosen such that each grid point corresponds to $64^3 = 262{,}144$ atoms after the finite difference discretization of the continuum mechanical system. We use $36^3 = 46{,}656$ grid points; hence the complete continuum system models $12{,}230{,}590{,}464$ atoms. For the time step, a value of $0.2\,\text{ps}$ turned out to be sufficient for stability. This is substantially larger than the time step size of $1\,\text{fs}$ which is usually used for atomistic simulations.

Figure 11 shows the results of the simulation at different time steps. The plots show a planar cross section through the specimen. The associated displacement of the specimen is visualized using a mesh. It is magnified by a factor of eight for better recognizability. The color indicates the velocity in the x_1-direction.

One can clearly observe how the system relaxes from its stressed initial configuration. The relaxation leads to eigenmode oscillations of the specimen. First, one can observe a basically circular movement of the whole inner part of the specimen. Later on, additional local oscillations with a higher frequency develop.

8. Conclusion. We proposed the inner expansion technique to derive quasi-continuum models from atomistic systems for crystalline solids. This approach is capable of capturing the material properties to a high extent, including those due to nonlinear deformations such as bending. In contrast to classical continuum limits, the discreteness effects of the underlying atomistic model are correctly reproduced. We showed this numerically for the simple model problem of an atomic chain. Unlike the direct expansion technique, which leads to a quasi-continuum description as well, our approach retains convexity of the atomistic potential. Therefore hyperbolicity and well-posedness of the resulting macroscopic evolution equations are guaranteed. Furthermore, we applied our new technique to a silicon crystal and showed that the higher approximation quality also holds for more complex potentials. Finally, we presented the results of a numerical simulation of its elastic response.

The main advantages of a quasi-continuum model compared to an atomistic model are as follows: Its numerical solution is much less costly, because the resolution of the discretization can be freely controlled, whereas the already discrete atomistic model is restricted to the physically given discreteness. This allows to use quite coarse grids for the discretization of the macroscopic model without losing its atomistic discreteness properties. Furthermore, much larger time step sizes than for the atomistic model can be used. Moreover, advanced numerical techniques such as adaptivity can be employed if necessary, and analytical techniques for PDEs might be applied. Finally, the rigorously derived higher order terms can be a good starting point to formulate improved phenomenological models, which capture the essential properties and coincide with the strictly derived ones to a good extent but might be easier to handle.

Furthermore, note that our method is also capable of reproducing boundary effects, i.e., the possibly different behavior of the specimen in the vicinity of its boundary. Although not exploited here, this can be important for potentials for which these effects play a substantial role. Such effects are lost with the scaling method, since the limiting procedure treats every inner point of the specimen as being surrounded by infinite bulk material, independently of its physical distance to the boundary.

Classical continuum mechanics deals with systems in the order of 10^{23} atoms for which the continuum limit often is a good description. But the advances in nanotech-
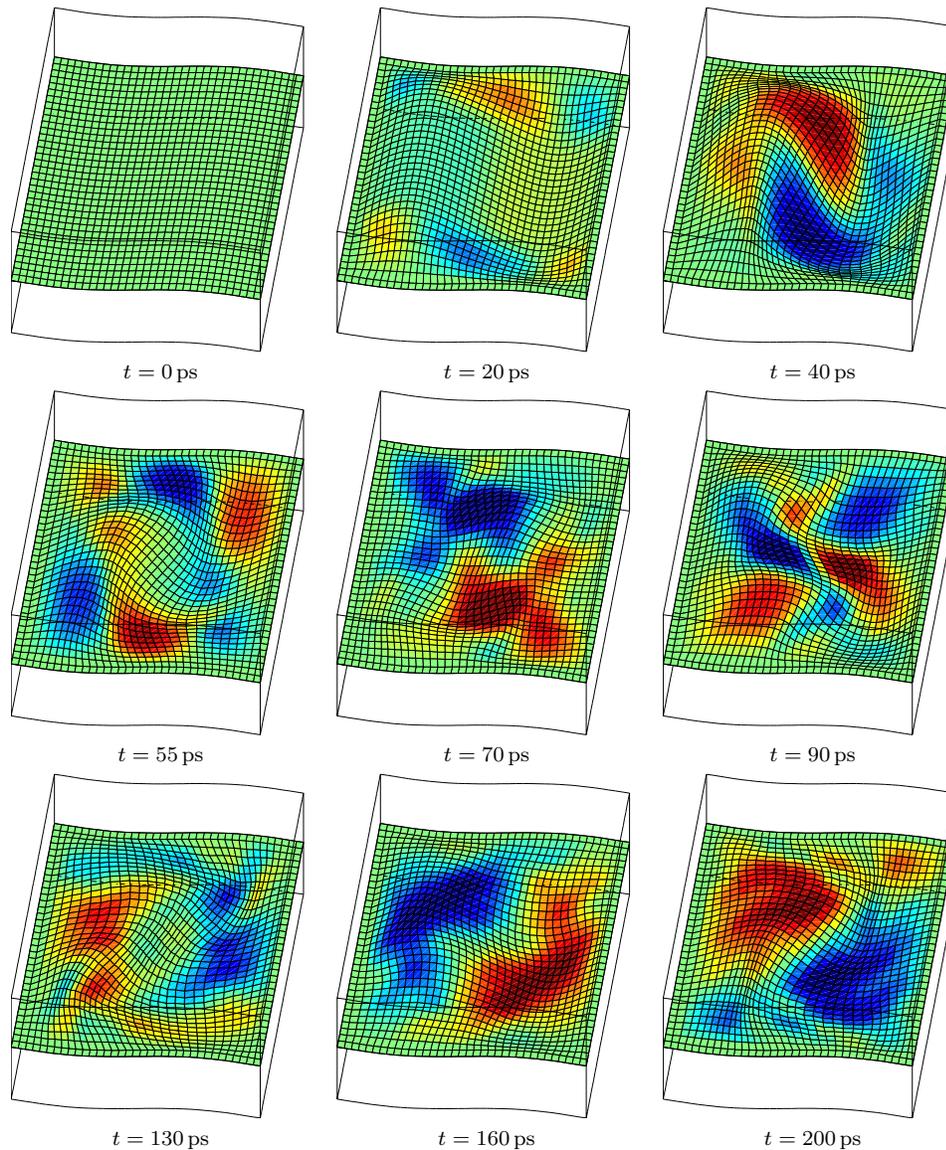
FIG. 11. *Elastic behavior of silicon. The cross section shows the displacement, magnified by the factor* 8. *The color denotes the velocity in the horizontally plotted* x_1*-direction.*

nology in recent years make it necessary to consider systems with a substantially smaller number of atoms for which the full continuum description clearly fails. On the other hand, these systems are still not in the reach of conventional molecular dynamics methods due to complexity reasons and the necessary small time step sizes involved. In this respect a quasi-continuum approach becomes more and more important also for practical applications. Here, a well-understood transition from the atomic level to the quasi-continuum level is essential for further developments towards multiscale simulations, bridging techniques, and similar approaches involving models on different scales; see, e.g., [30] and [35].

REFERENCES

[1] G. C. ABELL, *Empirical chemical pseudopotential theory of molecular and metallic bonding*, Phys. Rev. B, 31 (1985), pp. 6184–6196.

[2] E. C. AIFANTIS, *Update on a class of gradient theories*, Mech. Mater., 35 (2003), pp. 259–280.

[3] M. ARNDT, M. GRIEBEL, AND T. ROUBÍČEK, *Modelling and numerical simulation of martensitic transformation in shape memory alloys*, Contin. Mech. Thermodyn., 15 (2003), pp. 463–485.

[4] S. BARDENHAGEN AND N. TRIANTAFYLLIDIS, *Derivation of higher order gradient continuum theories in 2,3-D nonlinear elasticity from periodic lattice models*, J. Mech. Phys. Solids, 42 (1994), pp. 111–139.

[5] X. BLANC, C. LE BRIS, AND P.-L. LIONS, *From molecular models to continuum mechanics*, Arch. Ration. Mech. Anal., 164 (2002), pp. 341–381.

[6] R. BODENMANN, *Summation by Parts Formula for Noncentered Finite Differences*, Research Report 95-07, Seminar für Angewandte Mathematik, ETH Zürich, Zürich, Switzerland, 1995.

[7] M. BORN AND K. HUANG, *Dynamical Theory of Crystal Lattices*, Oxford University Press, New York, 1998.

[8] A. BRAIDES AND M. S. GELLI, *From Discrete to Continuum: A Variational Approach*, Lecture notes, SISSA, Trieste, Italy, 2000.

[9] D. W. BRENNER, *Empirical potential for hydrocarbons for use in simulating the chemical vapor deposition of diamond films*, Phys. Rev. B, 42 (1990), pp. 9458–9471.

[10] M. A. COLLINS, *A quasicontinuum approximation for solitons in an atomic chain*, Chem. Phys. Lett., 77 (1981), pp. 342–347.

[11] S. CURTAROLO AND G. CEDER, *Dynamics of an inhomogeneously coarse grained multiscale system*, Phys. Rev. Lett., 88 (2002), 255504.

[12] C. M. DAFERMOS, *Hyperbolic Conservation Laws in Continuum Physics*, Grundlehren Math. Wiss. 325, Springer, Berlin, 2000.

[13] M. S. DAW AND M. I. BASKES, *Semiempirical, quantum mechanical calculation of hydrogen embrittlement in metals*, Phys. Rev. Lett., 50 (1983), pp. 1285–1288.

[14] M. S. DAW AND M. I. BASKES, *Embedded-atom method: Derivation and application to impurities, surfaces, and other defects in metals*, Phys. Rev. B, 29 (1984), pp. 6443–6453.

[15] W. DREYER AND R. GUCKEL, *Micro-Macro Transitions by Interpolation, Smoothing/Averaging and Scaling of Particle Trajectories*, Preprint 725, WIAS Berlin, Berlin, Germany, 2002.

[16] W. E AND Z. HUANG, *A dynamic atomistic-continuum method for the simulation of crystalline materials*, J. Comput. Phys., 182 (2002), pp. 234–261.

[17] E. FERMI, J. PASTA, AND S. ULAM, *Studies of nonlinear problems* I, in Nonlinear Wave Motion, Lect. Appl. Math. 15, A. C. Newell, ed., AMS, Providence, RI, 1974, pp. 143–156.

[18] G. FRIESECKE AND R. D. JAMES, *A scheme for the passage from atomic to continuum theory for thin films, nanotubes and nanorods*, J. Mech. Phys. Solids, 48 (2000), pp. 1519–1540.

[19] G. FRIESECKE AND K. MATTHIES, *Geometric solitary waves in a 2D mass-spring lattice*, Discrete Contin. Dyn. Syst., 3 (2003), pp. 105–114.

[20] G. FRIESECKE AND R. L. PEGO, *Solitary waves on FPU lattices: I. Qualitative properties, renormalization and continuum limit*, Nonlinearity, 12 (1999), pp. 1601–1627.

[21] G. FRIESECKE AND F. THEIL, *Validity and failure of the Cauchy-Born hypothesis in a two-dimensional mass-spring lattice*, J. Nonlinear Sci., 12 (2002), pp. 445–478.

[22] P. G. KEVREKIDIS, I. G. KEVREKIDIS, A. R. BISHOP, AND E. S. TITI, *Continuum approach to discreteness*, Phys. Rev. E, 65 (2002), 046613.

[23] M. D. KRUSKAL AND N. J. ZABUSKY, *Stroboscopic perturbation procedure for treating a class of nonlinear wave equations*, J. Math. Phys., 5 (1964), pp. 231–244.

[24] P. ROSENAU, *Dynamics of nonlinear mass-spring chains near the continuum limit*, Phys. Lett. A, 118 (1986), pp. 222–227.

[25] P. ROSENAU, *Dynamics of dense lattices*, Phys. Rev. B, 36 (1987), pp. 5868–5876.

[26] P. ROSENAU, *Hamiltonian dynamics of dense chains and lattices: Or how to correct the continuum*, Phys. Lett. A, 311 (2003), pp. 39–52.

[27] J. ROWLINSON, *Translation of J. D. van der Waals' "The thermodynamic theory of capillarity under the hypothesis of a continuous variation of density,"* J. Stat. Phys., 20 (1979), pp. 197–244. English translation of [34].

[28] R. E. RUDD AND J. Q. BROUGHTON, *Coarse-grained molecular dynamics and the atomic limit of finite elements*, Phys. Rev. B, 58 (1998), pp. R5893–R5896.

[29] F. H. STILLINGER AND T. A. WEBER, *Computer simulation of local order in condensed phases of silicon*, Phys. Rev. B, 31 (1985), pp. 5262–5271.

[30] E. B. TADMOR, M. ORTIZ, AND R. PHILLIPS, *Quasicontinuum analysis of defects in solids*, Philos. Mag. A, 73 (1996), pp. 1529–1563.

[31] J. TERSOFF, *New empirical model for the structural properties of silicon*, Phys. Rev. Lett., 56 (1986), pp. 632–635.

[32] N. TRIANTAFYLLIDIS AND S. BARDENHAGEN, *On higher order gradient continuum theories in 1-D nonlinear elasticity. Derivation from and comparison to the corresponding discrete models*, J. Elasticity, 33 (1993), pp. 259–293.

[33] N. TRIANTAFYLLIDIS AND S. BARDENHAGEN, *The influence of scale size on the stability of periodic solids and the role of associated higher order gradient continuum models*, J. Mech. Phys. Solids, 44 (1996), pp. 1891–1928.

[34] J. D. VAN DER WAALS, *The thermodynamic theory of capillarity under the hypothesis of a continuous variation of density*, Verhandel. Konink. Akad. Weten. Amsterdam, 1 (1893), pp. 1–56 (in Dutch).

[35] G. J. WAGNER AND W. K. LIU, *Coupling of atomistic and continuum simulations using a bridging scale decomposition*, J. Comput. Phys., 190 (2003), pp. 249–274.

[36] J. A. D. WATTIS, *Approximations to solitary waves on lattices.* II. *Quasi-continuum methods for fast and slow waves*, J. Phys. A, 26 (1993), pp. 1193–1209.

[37] N. J. ZABUSKY AND M. D. KRUSKAL, *Interaction of "solitons" in a collisionless plasma and the recurrence of initial states*, Phys. Rev. Lett., 15 (1965), pp. 240–243.